

PAPER

Generalized hydrodynamics in box-ball system

To cite this article: Atsuo Kuniba *et al* 2020 *J. Phys. A: Math. Theor.* **53** 404001

View the [article online](#) for updates and enhancements.



IOP | ebooks™

Bringing together innovative digital publishing with leading authors from the global scientific community.

Start exploring the collection—download the first chapter of every title for free.

Generalized hydrodynamics in box-ball system

Atsuo Kuniba¹ , Grégoire Misguich^{2,3}  and Vincent Pasquier²

¹ Institute of Physics, University of Tokyo, Komaba, Tokyo 153-8902, Japan

² Institut de Physique Théorique, Université Paris Saclay, CEA, CNRS, F-91191 Gif-sur-Yvette, France

³ Laboratoire de Physique Théorique et Modélisation, CNRS UMR 8089, CY Cergy Paris Université, 95302 Cergy-Pontoise Cedex, France

E-mail: atsuo.s.kuniba@gmail.com, gregoire.misguich@ipht.fr and vincent.pasquier@ipht.fr

Received 16 April 2020, revised 4 August 2020

Accepted for publication 10 August 2020

Published 3 September 2020



CrossMark

Abstract

Box-ball system (BBS) is a prominent example of integrable cellular automata in one dimension connected to quantum groups, Bethe ansatz, ultradiscretization, tropical geometry and so forth. In this paper we study the generalized Gibbs ensemble of BBS soliton gas by thermodynamic Bethe ansatz and generalized hydrodynamics. The results include the solution to the speed equation for solitons, an intriguing connection of the effective speed with the period matrix of the tropical Riemann theta function, an explicit description of the density plateaux that emerge from domain wall initial conditions including their diffusive corrections.

Keywords: box-ball system, integrable cellular automata, solitons gas, generalized Gibbs ensemble, generalized hydrodynamics

(Some figures may appear in colour only in the online journal)

1. Introduction

The box-ball system (BBS) invented originally in [33] is an integrable cellular automaton on one dimensional lattice. It accommodates solitons exhibiting factorized scattering. Here is an example of collision of three solitons with amplitude 4, 2 and 1, where time evolution goes downward:

a quite general proof that the current by solitons coincides with the time average of the carrier current over the Poincaré cycle. This intriguing connection deserves a further investigation which we expect to yield a deeper insight into GHD.

We present a general formalism of the GHD [11] adapted to BBS. The essential variable is the occupation function, or equivalently the Y-function, in the TBA playing the role of the normal mode. As an application we study the non-equilibrium dynamics starting from domain wall initial conditions. It is a typical setting in the Riemann problem called *partitioning protocol*. Our numerical analysis demonstrates the formation of plateaux in the density profile after the evolution from the i.i.d. random initial states in the non-empty region. It testifies the ballistic transport of solitons where each plateau is filled with those having a selected list of amplitudes. The plateaux exhibit slight broadening in their edges due to the diffusive correction to the ballistic picture. A general recipe to calculate the diffusion constant for such a spread has been given in [9, 21]. We make use of these GHD machinery to derive an analytical formula for the positions and heights of the plateaux, and moreover the curves that describe their edge broadening. They agree with the numerical data excellently.

The layout of the paper is as follows. In section 2, we recall the basic features of BBS in the periodic boundary condition including commuting time evolutions T_1, T_2, \dots and a family of conserved quantities. In section 3, we study the GGE of BBS solitons by TBA. In particular for the two temperature case, closed formulas are given for the densities of strings, holes and the energies in (3.24)–(3.26). For the general case, the fugacity expansion solution is presented in appendix B. In section 4, we study the effective speed of solitons and the stationary current in the spatially homogeneous setting. Our speed equation (4.1) for the time evolution T_l coincides with [19, equation (11.7)] at $l = \infty$. It is established quite generally that the current due to solitons coincides with the time average of the carrier current [27, proposition 4.3]. The proof elucidates a new link between the effective speed and the period matrix B (4.6) which appeared originally in the tropical Riemann theta function [27, equation (4.14)]. For the two temperature GGE, the effective speed and the current are obtained in closed forms (D.2) and (D.3). The latter nontrivially agrees with an alternative derivation (E.20) based on a transfer matrix formalism. It also reproduces the earlier result in [6, lemma 3.15] for T_∞ . In section 5, we formulate GHD in a form adapted to BBS and apply it to the density plateaux generated from the domain wall initial conditions. We perform an extensive numerical analysis and confirm an agreement with high accuracy. Section 6 contains a future outlook concerning a more general BBS. Appendix A presents a transfer matrix formalism of the GGE partition function. Appendix B relates the TBA equation to the generalized Q-system and provides the multi-fugacity series expansion formulas. Appendix C provides a proof of (4.14) which leads to the general formula (4.19) of the effective speed in terms of the hole density. Appendices D and E derive an explicit formula for the current in homogeneous case by two different methods. Appendix F recalls the linearly degenerate hydrodynamic type systems from [24, 35].

2. Box–ball system

In this section we recall the basic features of the generalized periodic BBS equipped with commuting time evolutions T_1, T_2, \dots [28] which includes T_∞ studied in [37].

2.1. Combinatorial R

For a positive integer l , set $B_l = \{(x_0, x_1) \in (\mathbb{Z}_{\geq 0})^2 \mid x_0 + x_1 = l\}$. We shall use \otimes to denote the product of the sets B_l 's and their elements instead of \times having the crystal structure in mind although its consequence will not be utilized explicitly in this paper. Define a map $R_{l,m} : B_l \otimes B_m \rightarrow B_m \otimes B_l$ by

$$R_{l,m}: (x_0, x_1) \otimes (y_0, y_1) \mapsto (\tilde{y}_0, \tilde{y}_1) \otimes (\tilde{x}_0, \tilde{x}_1), \tag{2.1}$$

$$\begin{aligned} \tilde{x}_i &= x_i + \min(x_{i+1}, y_i) - \min(x_i, y_{i+1}), \\ \tilde{y}_i &= y_i - \min(x_{i+1}, y_i) + \min(x_i, y_{i+1}), \end{aligned} \tag{2.2}$$

where all the indices are in \mathbb{Z}_2 . The map $R_{l,m}$ is known as the combinatorial R of $A_1^{(1)}$. It is a bijection and satisfies the inversion relation $R_{l,m}R_{m,l} = \text{id}_{B_m \otimes B_l}$ and the Yang–Baxter relation $(1 \otimes R_{k,l})(R_{k,m} \otimes 1)(1 \otimes R_{l,m}) = (R_{l,m} \otimes 1)(1 \otimes R_{k,m})(R_{k,l} \otimes 1)$. It also enjoys the symmetry corresponding to the Dynkin diagram automorphism of $A_1^{(1)}$:

$$R(\omega \otimes \omega) = (\omega \otimes \omega)R, \quad \omega((x_0, x_1)) = (x_1, x_0). \tag{2.3}$$

The BBS considered in this paper is mostly concerned with $R_{l,1} : B_l \otimes B_1 \rightarrow B_1 \otimes B_l$. Its action is given by $(l - n, n) \otimes (1 - \eta, \eta) \mapsto (1 - \tilde{\eta}, \tilde{\eta}) \otimes (l - \tilde{n}, \tilde{n})$, where $\tilde{\eta}, \tilde{n}$ are determined from n, η according to the following diagrams:

$$\begin{array}{ccc} \begin{array}{c} \eta \\ | \\ n \text{---} \rightarrow \tilde{n} \\ | \\ \tilde{\eta} \end{array} & = & \begin{array}{c} 0 \\ | \\ n \text{---} \rightarrow n-1 \\ | \\ 1 \end{array} \quad (n > 0) \qquad \begin{array}{c} 0 \\ | \\ 0 \text{---} \rightarrow 0 \\ | \\ 0 \end{array} \\ & & \begin{array}{c} 1 \\ | \\ n \text{---} \rightarrow n+1 \\ | \\ 0 \end{array} \quad (n < l) \qquad \begin{array}{c} 1 \\ | \\ l \text{---} \rightarrow l \\ | \\ 1 \end{array} \end{array} \tag{2.4}$$

2.2. States, time evolutions and energies

The BBS is a dynamical system on a periodic lattice of size L . An element $\eta = \eta_1 \otimes \dots \otimes \eta_L \in B_1^{\otimes L}$ is called a state. In what follows a local state $(1 - \eta_i, \eta_i) \in B_1$ is flexibly identified with $\eta_i \in \{0, 1\}$ and interpreted as a box containing η_i balls at site $i \in \mathbb{Z}_L$. Thus the state η is also presented as an array $\eta = (\eta_1, \dots, \eta_L) \in \{0, 1\}^L$.

In order to introduce the time evolution, consider the composition of $R_{l,1}$ L times which sends $B_l \otimes B_1^{\otimes L}$ to $B_1^{\otimes L} \otimes B_l$. If $\xi_l \otimes \eta_1 \otimes \dots \otimes \eta_L \mapsto \tilde{\eta}_1 \otimes \dots \otimes \tilde{\eta}_L \otimes \tilde{\xi}_l$ under this map, the situation is depicted as a concatenation of the diagrams (2.4) in the form of a row transfer matrix:

$$\begin{array}{ccccccc} & \eta_1 & \eta_2 & \dots & \eta_{L-1} & \eta_L & \\ \xi_l & \downarrow & \downarrow & \dots & \downarrow & \downarrow & \rightarrow \tilde{\xi}_l \\ & \tilde{\eta}_1 & \tilde{\eta}_2 & \dots & \tilde{\eta}_{L-1} & \tilde{\eta}_L & \end{array} \tag{2.5}$$

As with η_i , we identify the elements $(l - n, n) \in B_l$ attached to the horizontal line with $n \in \{0, 1, \dots, l\}$, and regard it as the capacity l carrier containing n balls [32]. In this interpretation, the diagrams (2.4) for $R_{l,1}$ describe a loading/unloading process of balls between a local box and the capacity l carrier which is proceeding to the right.

Given $\xi_l \in B_l$ and $\eta = (\eta_1, \dots, \eta_L)$, the diagram (2.5) determines $\tilde{\eta} = (\tilde{\eta}_1, \dots, \tilde{\eta}_L)$ and $\tilde{\xi}_l \in B_l$ uniquely. This relation will be expressed as⁵ $\xi_l \otimes \eta \simeq \tilde{\eta} \otimes \tilde{\xi}_l$.

⁵ We use \simeq to signify that the RHS is actually the result of successive application of $R_{l,1}$ to the LHS bearing in mind that it causes the isomorphism of crystals $B_l \otimes B_1^{\otimes L} \simeq B_1^{\otimes L} \otimes B_l$.

$[L/2]$ is equivalent and allows all the possible amplitude for the solitons. See [28, equations (3.6) and (4.21)] for the precise description.

Example 3.1. Consider $L = 9$, $m = (m_1, m_2, m_3, \dots) = (1, 0, 1, 0, 0, \dots)$, hence $(p_1, p_2, p_3, \dots) = (5, 3, 1, 1, \dots)$. For $s \geq 3$, the iso-level set $\mathcal{P}_s(m)$ consists of the 45 states given by the \mathbb{Z}_9 cyclic shifts of

$$(000010111), (000100111), (001000111), (010000111), (000011011),$$

where the last one is the ‘intermediate’ state during the collision in which amplitude $3 + 1$ temporarily look $2 + 2$. The cardinality is reproduced as $|\mathcal{P}_s(m)| = \frac{9}{9-8} \binom{5}{1} \binom{3}{0} \binom{1}{1} = 45$.

Example 3.2. Consider example 2.4, which corresponds to $L = 19$ and $m = (m_1, m_2, m_3, \dots) = (2, 2, 1, 0, 0, \dots)$, hence $(p_1, p_2, p_3, \dots) = (9, 3, 1, 1, 1, \dots)$. Thus (3.3) with any $s \geq 3$ gives

$$|\mathcal{P}_s(m)| = \frac{19}{1} \binom{10}{2} \binom{4}{2} \binom{1}{1} = 10\,260. \quad (3.4)$$

3.2. Generalized Gibbs ensemble

We are going to study the gas of BBS solitons with amplitude not exceeding s in terms of the generalized Gibbs ensemble involving the energies E_1, E_2, \dots, E_s with the conjugate inverse temperatures $\beta_1, \beta_2, \dots, \beta_s$. It will be referred to as $\text{GGE}(\beta_1, \beta_2, \dots, \beta_s)$. The canonical partition function reads

$$Z_L(\beta_1, \dots, \beta_s) = \sum_{\eta} e^{-\beta_1 E_1 - \dots - \beta_s E_s} \quad (3.5)$$

with the sum taken over $\eta \in \{0, 1\}^L$ such that $m_j = 0$ for $j > s$. The free energy per site is

$$\mathcal{F} = -\lim_{L \rightarrow \infty} \frac{1}{L} \log Z_L(\beta_1, \dots, \beta_s) \quad (3.6)$$

$$= -\lim_{L \rightarrow \infty} \frac{1}{L} \log \left(\sum_m |\mathcal{P}_s(m)| e^{-\sum_{1 \leq j, k \leq s} \beta_j \min(j, k) m_k} \right), \quad (3.7)$$

where the sum is taken with respect to $m = (m_1, \dots, m_s) \in (\mathbb{Z}_{\geq 0})^s$. To get the second line, we used the fact that the inclusion of the contributions from those η such that $M \geq L/2$ in (3.5) at most doubles the quantity in log by remark 2.1. In appendix A, we present a transfer matrix formalism of the partition function (3.5), which formally corresponds to the maximal choice $s = [L/2]$. It enables us to compute the free energy \mathcal{F} . However to compute the current, we actually need a more refined information on the density on solitons with each amplitude (see appendix E for an approach to bypass it at least for the two temperature GGE). To extract it, we resort to the thermodynamic Bethe ansatz in the next subsection.

3.3. Thermodynamic Bethe ansatz

Assuming the L -linear scaling

$$m_j \simeq L\rho_j, \quad p_j \simeq L\sigma_j, \quad E_j \simeq L\varepsilon_j, \quad (3.8)$$

$$\varepsilon_j = \sum_{k=1}^s \min(j, k) \rho_k, \quad \sigma_j = 1 - 2\varepsilon_j, \quad (3.9)$$

and substituting (3.3) into (3.7), we find

$$\mathcal{F} = \beta_1 \varepsilon_1 + \dots + \beta_s \varepsilon_s - \sum_{i=1}^s ((\sigma_i + \rho_i) \log(\sigma_i + \rho_i) - \sigma_i \log \sigma_i - \rho_i \log \rho_i), \quad (3.10)$$

where ρ_i is the solution to the condition $\frac{\partial \mathcal{F}}{\partial \rho_i} = 0$. It leads to the TBA equation:

$$\sum_{j=1}^s \min(i, j) \beta_j = \log(1 + Y_i) - 2 \sum_{j=1}^s \min(i, j) \log(1 + Y_j^{-1}), \quad Y_i = \frac{\sigma_i}{\rho_i}. \quad (3.11)$$

It is cast into the (constant) Y-system:

$$Y_1^2 = e^{\beta_1} (1 + Y_2), \quad (3.12)$$

$$Y_i^2 = e^{\beta_i} (1 + Y_{i-1})(1 + Y_{i+1}) \quad (1 < i < s), \quad (3.13)$$

$$Y_s^2 = e^{\beta_s} (1 + Y_{s-1})(1 + Y_s). \quad (3.14)$$

Note the irregularity of the very last factor which is *not* $1 + Y_{s+1}$. In terms of the positive solution Y_1, \dots, Y_s to the Y-system, the free energy (3.6) is given by

$$\mathcal{F} = - \sum_{i=1}^s \log(1 + Y_i^{-1}). \quad (3.15)$$

In appendix B we present low temperature series expansions for \mathcal{F}, Y_i, ρ_i and ε_i , etc.

3.4. Two temperature GGE

In this subsection we focus on the special case $GGE(\beta_1, \beta_\infty)$ including the two inverse temperatures β_1 and β_∞ . Their conjugate energies E_1 and E_∞ are the only cases that become sums of *local* correlations. See (2.10) and (2.13).

Consider the Y-system (3.12)–(3.14) with $\beta_2 = \dots = \beta_{s-1} = 0$. It is equivalent to the following equations and the boundary condition:

$$Y_i^2 = (1 + Y_{i-1})(1 + Y_{i+1}) \quad (1 \leq i \leq s), \quad (3.16)$$

$$1 + Y_0 = e^{\beta_1}, \quad 1 + Y_{s+1} = e^{\beta_s} (1 + Y_s). \quad (3.17)$$

An advantage of (3.16) over (3.13) is that it allows a general solution simply expressible in terms of two parameters a, z :

$$Y_i = Q_{i-1} Q_{i+1}, \quad Q_i = \frac{a^{\frac{1}{2}} z^{\frac{i}{2}} - a^{-\frac{1}{2}} z^{-\frac{i}{2}}}{z^{\frac{1}{2}} - z^{-\frac{1}{2}}}, \quad (3.18)$$

where the latter satisfies another difference equation called Q-system:

$$Q_i^2 = Q_{i-1} Q_{i+1} + 1 \quad (i \in \mathbb{Z}). \quad (3.19)$$

Moreover, the boundary condition (3.17) relates a, z to the temperatures as

$$e^{\frac{\beta_1}{2}} = Q_0 = \frac{a^{\frac{1}{2}} - a^{-\frac{1}{2}}}{z^{\frac{1}{2}} - z^{-\frac{1}{2}}}, \quad e^{\beta_s} = \left(\frac{Q_{s+1}}{Q_s} \right)^2 \xrightarrow{s \rightarrow \infty} e^{\beta_\infty} = z^{-1}, \quad (3.20)$$

where we have assumed $0 < z < 1$ without loss of generality to derive the latter relation. On the other hand the first relation demands $0 < a \leq z$ in order to satisfy $\beta_1 \geq 0$.

The free energy (3.15) is evaluated as

$$\mathcal{F} = -\sum_{i=1}^s \log\left(\frac{Q_i^2}{Q_{i-1}Q_{i+1}}\right) = \log\left(\frac{Q_0Q_{s+1}}{Q_1Q_s}\right) \xrightarrow{s \rightarrow \infty} \log\left(\frac{1-a}{1-az}\right). \quad (3.21)$$

From \mathcal{F} , the expectation values of the energy densities ε_1 and ε_∞ are derived as

$$\varepsilon_1 = \frac{\partial \mathcal{F}}{\partial \beta_1} = \left(\frac{\partial a}{\partial \beta_1} \frac{\partial}{\partial a} + \frac{\partial z}{\partial \beta_1} \frac{\partial}{\partial z}\right) \mathcal{F} = -\frac{a(1-a)}{1+a} \frac{\partial}{\partial a} \mathcal{F} = \frac{a(1-z)}{(1+a)(1-az)}, \quad (3.22)$$

$$\varepsilon_\infty = \frac{\partial \mathcal{F}}{\partial \beta_\infty} = \left(\frac{\partial a}{\partial \beta_\infty} \frac{\partial}{\partial a} + \frac{\partial z}{\partial \beta_\infty} \frac{\partial}{\partial z}\right) \mathcal{F} = \left(-\frac{a(1-a)(1+z)}{(1+a)(1-z)} \frac{\partial}{\partial a} - z \frac{\partial}{\partial z}\right) \mathcal{F} = \frac{a}{1+a}, \quad (3.23)$$

where the latter is the total density of balls due to (2.13). Note that ε_∞ is not $\frac{z}{1+z}$ despite that $z = e^{-\beta_\infty}$ from (3.20).

So far, we have solved the Y-system (3.16) and (3.17). The remaining task is to find $\varepsilon_j, \rho_j, \sigma_j$ satisfying (3.9), $\sigma_i/\rho_i = Y_i$ (3.11) and the boundary condition (3.22) and (3.23) in the limit $s \rightarrow \infty$. The answer is given by

$$\varepsilon_i = \frac{a(1-z^i)}{(1+a)(1-az^i)}, \quad (3.24)$$

$$\sigma_i = \frac{(1-a)(1+az^i)}{(1+a)(1-az^i)}, \quad (3.25)$$

$$\rho_i = \frac{az^{i-1}(1-a)(1-z)^2(1+az^i)}{(1+a)(1-az^{i-1})(1-az^i)(1-az^{i+1})}. \quad (3.26)$$

The result (3.25) reduces to $\varphi_1^{(1)}|_{\kappa=1}$ in [25, equation (182)] when $a = z = q$, where q is the parameter such that the ball density becomes $\frac{q}{1+q}$ for the single color case in [25]. In view of (3.20), it corresponds to $\beta_1 = 0$ which is the Gibbs ensemble with the single inverse temperature β_∞ . This is the unique case in which the probability distribution of the BBS local states η_i becomes i.i.d. in which the relative probability is given by $\mathbb{P}(\eta_i = 1)/\mathbb{P}(\eta_i = 0) = z$.

4. Stationary current

4.1. Effective speed of solitons

Consider the BBS with time evolution T_l as a gas of solitons. Each soliton is subject to the interaction with the others via collisions. As explained along examples 2.2 and 2.3, an i -soliton has the bare speed $\min(i, l)$ and acquires the phase shift $2 \min(i, k)$ in its trajectory by a collision with a k -soliton. Let $v_i^{(l)}$ denote the effective speed of i -solitons under T_l . Then the above features of the soliton interaction lead to the consistency condition [14, 19, 38]:

$$v_i^{(l)} = \min(i, l) + 2 \sum_{k=1}^{\infty} \min(i, k)(v_i^{(l)} - v_k^{(l)})\rho_k \quad (\forall i \geq 1), \quad (4.1)$$

where ρ_k is the density of k -solitons. The first term on the RHS is the bare speed and the second term takes the interaction effect into account. A speed equation of this kind has been postulated

in the generalized hydrodynamics [13, equation (7)]. In particular (4.1) reduces to [19, equation (11.7)] as $l \rightarrow \infty$.

By the definition, the current $J^{(l)}$ in our BBS is the number of balls passing through a site to the right by applying T_l once. It consists of contributions from i -solitons for any $i \geq 1$ as

$$J^{(l)} = \sum_{i=1}^{\infty} i \rho_i v_i^{(l)}, \tag{4.2}$$

where the effective speed $v_i^{(l)}$ should be determined from (4.1) for a given density distribution $(\rho_k)_{k \geq 1}$. This formula corresponds to [11, equation (3.62)].

4.2. Coincidence with time average

As demonstrated in example 2.4, balls in a BBS state are moved to the right periodically by a carrier of capacity l under the time evolution T_l . Thus the stationary current $J^{(l)}$ (4.2) based on the soliton picture should coincide with the *time average* $\bar{J}^{(l)}$ of the number of balls in the carrier over the *Poincaré cycle* of a given BBS state. An explicit formula of $\bar{J}^{(l)}$ has been obtained in [27] by a calculation involving a tropical (or ultradiscrete) analogue of the Riemann theta function. In this subsection we prove

$$J^{(l)} = \bar{J}^{(l)} \tag{4.3}$$

quite generally without recourse to a specific choice of the soliton densities $(\rho_k)_{k \geq 1}$. By so doing we will illuminate an intriguing connection between the effective speed and the period matrix of the tropical Riemann theta function [27, equation (4.14)]. The latter has emerged from the Bethe ansatz at $q = 0$. Its application to the BBS has revealed the Bethe roots at $q = 0$ as action-angle variables, Bethe eigenvalues at $q = 0$ giving the Poincaré cycle, torus decomposition interpretation of a Fermionic character formula, multiplicity formula of the invariant torus and explicit solution of the initial value problem in terms of tropical Riemann theta functions and so forth [27, 28].

4.2.1. Time averaged current and topological period matrix. The time average $\bar{J}^{(l)}$ for a given state η has been obtained in [27, proposition 4.3]. It is independent of the position and expressed in terms of the data determined from the conserved Young diagram $Y(\eta)$ (2.12) as

$$\bar{J}^{(l)} = \hat{\kappa}^{(\infty)\top} B^{-1} \hat{\kappa}^{(l)}. \tag{4.4}$$

This was the first nontrivial dynamical characteristic of the BBS derived from an explicit calculation using the tropical Riemann theta function. To explain the RHS of (4.4), let m_i be the number of i -solitons and assume the same notations for the vacancy p_i (3.1) and the densities ρ_i, σ_i (3.8) as before. Let s be the width of the Young diagram $Y(\eta)$ (2.12), i.e., the amplitude of the largest solitons. Denote the depth of $Y(\eta)$ by $g = E_1 = m_1 + \dots + m_s$. Thus in particular the vacancy (3.1) reads

$$p_j = L - 2 \sum_{k=1}^s \min(j, k) m_k \quad (j \geq 0), \tag{4.5}$$

where we have introduced the upper bound s . This satisfies $L = p_0 > p_1 > \dots > p_s = \dots = p_\infty = L - 2M \geq 1$.

Now B and $\hat{\kappa}^{(l)}$ are a g -dimensional matrix and a column vector possessing the block structure as follows [27, equation (4.27)]:

$$B = \begin{pmatrix} B_{11} & \cdots & B_{1s} \\ \vdots & \ddots & \vdots \\ B_{s1} & \cdots & B_{ss} \end{pmatrix}, \tag{4.6}$$

$$B_{ij} = (\delta_{ij}\delta_{\alpha\beta}p_i + 2 \min(i, j))_{1 \leq \alpha \leq m_i, 1 \leq \beta \leq m_j} \in \text{Mat}(m_i, m_j),$$

$$\hat{\kappa}^{(l)} = (\kappa_i^{(l)})_{1 \leq i \leq s, 1 \leq \alpha \leq m_i} \in (\mathbb{Z}_{>0})^g, \quad \kappa_i^{(l)} = \min(i, l). \tag{4.7}$$

The matrix B is the tropical analogue of the period matrix of the Riemann theta function and $\hat{\kappa}^{(l)}$ is the velocity vector of the angle variables in the Jacobi variety on which the dynamics becomes a straight motion [27, 28].⁶ The vector $\hat{\kappa}^{(\infty)T}$ in (4.4) denotes the transpose of the column vector $\hat{\kappa}^{(\infty)}$.

Example 4.1. Consider the case $m_1 = m_2 = m_3 = 2$ ($s = 3, g = 6$). Then B [27, equation (4.6)] is a 6×6 matrix and $\hat{\kappa}^{(l)}$ is a 6-dimensional row vector given by

$$B = \begin{pmatrix} p_1 + 2 & 2 & 2 & 2 & 2 & 2 \\ 2 & p_1 + 2 & 2 & 2 & 2 & 2 \\ 2 & 2 & p_2 + 4 & 4 & 4 & 4 \\ 2 & 2 & 4 & p_2 + 4 & 4 & 4 \\ 2 & 2 & 4 & 4 & p_3 + 6 & 6 \\ 2 & 2 & 4 & 4 & 6 & p_3 + 6 \end{pmatrix}, \tag{4.8}$$

$$\hat{\kappa}^{(l)T} = (\min(l, 1), \min(l, 1), \min(l, 2), \min(l, 2), \min(l, 3), \min(l, 3)). \tag{4.9}$$

Example 4.2. For examples 2.4 and 3.2, we have

$$B = \begin{pmatrix} 11 & 2 & 2 & 2 & 2 \\ 2 & 11 & 2 & 2 & 2 \\ 2 & 2 & 7 & 4 & 4 \\ 2 & 2 & 4 & 7 & 4 \\ 2 & 2 & 4 & 4 & 7 \end{pmatrix}, \quad \hat{\kappa}^{(1)} = \begin{pmatrix} 1 \\ 1 \\ 1 \\ 1 \\ 1 \end{pmatrix}, \quad \hat{\kappa}^{(2)} = \begin{pmatrix} 1 \\ 1 \\ 2 \\ 2 \\ 2 \end{pmatrix}, \quad \hat{\kappa}^{(l)} = \begin{pmatrix} 1 \\ 1 \\ 2 \\ 2 \\ 3 \end{pmatrix} \quad (l \geq 3). \tag{4.10}$$

4.2.2. Inverse of tropical period matrix. To elucidate the connection to the speed equation, our first task is to compute the inverse $X = B^{-1}$. It turns out that X also has the same block structure as B :

$$X = \begin{pmatrix} X_{11} & \cdots & X_{1s} \\ \vdots & \ddots & \vdots \\ X_{s1} & \cdots & X_{ss} \end{pmatrix}, \tag{4.11}$$

$$X_{ij} = (\delta_{ij}\delta_{\alpha\beta}p_i^{-1} + x_{\min(i,j)})_{1 \leq \alpha \leq m_i, 1 \leq \beta \leq m_j} \in \text{Mat}(m_i, m_j).$$

⁶It was denoted by \mathbf{h}_l in [27, equation (4.27)].

The condition $\sum_{j=1}^s B_{ij} X_{jk} = \delta_{ik} \text{id}_{m_i}$ reads, in terms of the parameters x_1, \dots, x_s , as

$$p_i x_{\min(i,j)} + 2 \min(i, j) p_j^{-1} + 2 \sum_{k=1}^s \min(i, k) m_k x_{\min(j,k)} = 0 \quad (1 \leq i, j \leq s). \tag{4.12}$$

For instance when $s = 4$, it can be presented in a matrix form:

$$\begin{aligned} & \begin{pmatrix} p_1 + 2m_1 & 2m_2 & 2m_3 & 2m_4 \\ 2m_1 & p_2 + 4m_2 & 4m_3 & 4m_4 \\ 2m_1 & 4m_2 & p_3 + 6m_3 & 6m_4 \\ 2m_1 & 4m_2 & 6m_3 & p_4 + 8m_4 \end{pmatrix} \begin{pmatrix} x_1 & x_1 & x_1 & x_1 \\ x_1 & x_2 & x_2 & x_2 \\ x_1 & x_2 & x_3 & x_3 \\ x_1 & x_2 & x_3 & x_4 \end{pmatrix} \\ &= -2 \begin{pmatrix} p_1^{-1} & p_2^{-1} & p_3^{-1} & p_4^{-1} \\ p_1^{-1} & 2p_2^{-1} & 2p_3^{-1} & 2p_4^{-1} \\ p_1^{-1} & 2p_2^{-1} & 3p_3^{-1} & 3p_4^{-1} \\ p_1^{-1} & 2p_2^{-1} & 3p_3^{-1} & 4p_4^{-1} \end{pmatrix}. \end{aligned} \tag{4.13}$$

In appendix C, we prove that the over-determined s^2 equation (4.12) on x_1, \dots, x_s admits the unique solution:

$$x_k = - \sum_{j=1}^k \frac{2}{p_{j-1} p_j}. \tag{4.14}$$

4.2.3. Speed equation as inversion of tropical period matrix. By substituting (4.5) into the first term of (4.12) with j replaced by l , we have

$$L x_{\min(i,l)} = - \frac{2 \min(i, l)}{p_l} + 2 \sum_{k=1}^s \min(i, k) (x_{\min(i,l)} - x_{\min(l,k)}) m_k. \tag{4.15}$$

Further substituting the scaling forms (3.8) and

$$x_k \simeq L^{-2} \nu_k \tag{4.16}$$

and taking the limit $L, s \rightarrow \infty$ we get

$$\nu_{\min(i,l)} = - \frac{2 \min(i, l)}{\sigma_l} + 2 \sum_{k=1}^{\infty} \min(i, k) (\nu_{\min(i,l)} - \nu_{\min(l,k)}) \rho_k \quad (\forall i, l \geq 1). \tag{4.17}$$

Comparing this with (4.1), we find that the speed $v_i^{(l)}$ of i -solitons under T_l is given by

$$v_i^{(l)} = - \frac{\sigma_l}{2} \nu_{\min(i,l)} = \frac{\sigma_l}{\sigma_\infty} v_{\min(i,l)}, \quad v_i := v_i^{(\infty)} = - \frac{\sigma_\infty}{2} \nu_i. \tag{4.18}$$

Thus the effective speed of solitons can essentially be identified with appropriately scaled elements of the inverse tropical period matrix. Our subsequent proof of (4.4) in section 4.2.4 will further demonstrate this fact somewhat more directly.

Combining (4.14), (4.16) and (4.18) we discover the general relation connecting the effective speed and the hole density ($\sigma_0 = 1$):

$$v_k^{(l)} = \sum_{j=1}^{\min(k,l)} \frac{\sigma_l}{\sigma_{j-1} \sigma_j}, \quad v_k = \sum_{j=1}^k \frac{\sigma_\infty}{\sigma_{j-1} \sigma_j}. \tag{4.19}$$

We note that these are formally exact even for *finite* L provided that all the \simeq in (3.8) and (4.16) are replaced by the equality.

In appendix D, we evaluate this sum for (3.25) to obtain the effective speed and the current explicitly in $\text{GGE}(\beta_1, \beta_\infty)$. The result are (D.2) and (D.3). In appendix E, we further confirm the result by a transfer matrix method.

4.2.4. Proof of (4.3). Given a column vector $\xi = (\xi_i) = (\xi_1, \xi_2, \dots)^T$ whose components are labeled by soliton amplitude i , we denote its m_i -fold duplication for each i by attaching hat as

$$\hat{\xi} = (\overbrace{\xi_1, \dots, \xi_1}^{m_1}, \overbrace{\xi_2, \dots, \xi_2}^{m_2}, \dots)^T. \tag{4.20}$$

This convention matches the notation in (4.7). Note that the speed equation (4.1) is expressed by using the vacancy $p_i = L - 2 \sum_j \min(i, j) m_j$ as

$$p_i v_i^{(l)} + \sum_j 2 \min(i, j) v_j^{(l)} m_j = L \hat{\kappa}_i^{(l)}. \tag{4.21}$$

Recalling that $B = (\delta_{ij} \delta_{\alpha\beta} p_i + 2 \min(i, j))_{i\alpha, j\beta}$ (4.6), the equation (4.21) is written in the matrix form

$$B \hat{v}^{(l)} = L \hat{\kappa}^{(l)}. \tag{4.22}$$

On the other hand the soliton current density is

$$J^{(l)} = \sum_i i \rho_i v_i^{(l)} = \frac{1}{L} \sum_i i m_i v_i^{(l)} = \frac{1}{L} \hat{\kappa}^{(\infty)T} \cdot \hat{v}^{(l)}. \tag{4.23}$$

Thus we have the equality with the time average as

$$J^{(l)} = \frac{1}{L} \hat{\kappa}^{(\infty)T} \cdot L B^{-1} \hat{\kappa}^{(l)} = \hat{\kappa}^{(\infty)T} \cdot B^{-1} \hat{\kappa}^{(l)} = \bar{J}^{(l)}. \tag{4.24}$$

It will be interesting to extend the result of this subsection to the periodic box-ball system with n kinds of balls [27]. In fact, most of the necessary ingredients have already been formulated universally in terms of the Bethe ansatz and the root system associated with $A_n^{(1)}$ including the time averaged current [27, proposition 4.4] and the tropical period matrix [27, equation (4.6)].

5. Domain wall problem and generalized hydrodynamics

In this section we discuss the dynamics of the BBS model when the system is initially prepared in an inhomogeneous state. We consider in particular a family of domain-wall problems with different ball densities in the ‘left’ and in the ‘right’ halves of the system.

To be precise, at time $t = 0$, in the ‘left’ half of the system (from site $r = -L/2$ to $r = 0$), we have, on each site, a ball with probability p_L and an empty site with probability $1 - p_L$. In term of fugacity, we have $z_L : p_L = z_L / (1 + z_L)$. Similarly, in the ‘right’ half (from site $r = 1$ to $r = L/2 - 1$) the ball density is p_R . So, each half of the system is thus initially prepared in a one-temperature GGE state. Next we evolve, using T_l with carrier capacity l , and mainly investigate the evolution of the ball density $h^{(l)}(r, t)$ at site r and time t , averaged over a large number of initial states.

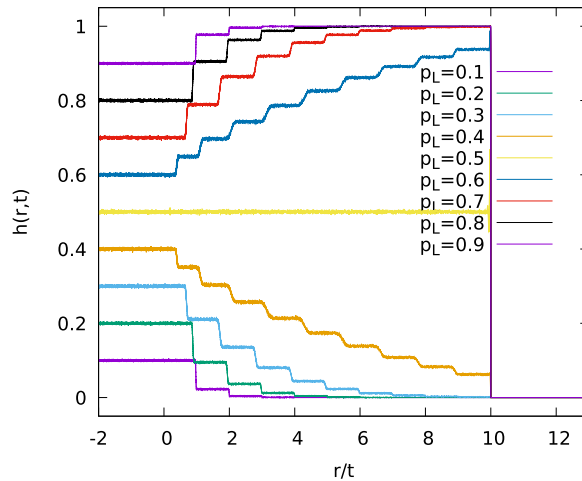


Figure 1. Ball density plotted as a function $\zeta = r/t$ for different initial ball densities p_L in the left half of the system. The right half is initially empty, $p_R = 0$, and $l = 10$. For each density p two curves are plotted, corresponding to $t = 500$ and $t = 1000$. Both curves turn out to be almost on top of each other. The density vanishes for $\zeta > l = 10$, which corresponds to the fastest velocity in this problem. Note that for $\zeta < l$ the curves associated to p and $1 - p$ are symmetric with respect to $h = 1/2$ (see remark 2.1).

We present data for $l = 2, 3, 4, 10, 20$ and 100 , and simulations carried out up to $t = 2000$. Unless specified otherwise the simulations have been performed with $N_{\text{samples}} = 5 \times 10^4$ random initial conditions and a system size $L = 10^5$. In a few cases, to increase the precision, we pushed the simulations to $N_{\text{samples}} = 10^6$ and $L = 10^6$. The systems we simulate are sufficiently large, so that, in the time range we consider the ‘wrapping effect’ on the periodic ring does not play any role and we are therefore effectively dealing with the *infinite* system.

The figure 1 represents the ball density $h^{(l)}(r, t)$ for an initial state with densities $p_R = 0$, various values of p_L , and $l = 10$. When plotted as a function of $\zeta = r/t$, the data associated to different times t practically collapse onto a single curve and these density profiles show some marked plateaux. As we will discuss in the following paragraphs, this can be understood and described analytically in terms of generalized hydrodynamics (GHD) [2, 5, 11–13] (see also [15, 16]) adapted to the BBS. We also note that a similar domain-wall problem for a classical integrable model of hard-rods has been recently solved using GHD [12].

The central idea is to assume that the system can locally, at some Euler scale, be described by soliton densities ρ_j and effective velocities v_j related through (5.2). The evolution in space and time of these quantities is then obtained by imposing the conservation of each soliton species (see (5.16) and (5.17)).

5.1. Densities and velocities

We first introduce some notations: if v is a vector, each entry v_k being associated to one soliton size, we denote $\mathbf{v}_{kl} = v_k \delta_{kl}$ the corresponding diagonal matrix. If v, w are vectors we denote by $v * w$ the vector with components $(v * w)_k = v_k w_k$. It is also equal to $v * w = \mathbf{v}w = w * v$. Also, $\mathbf{v}^{-1}w = w/v$. Note that for a matrix M , in general $(Ma) * b \neq M(a * b)$ unless M is diagonal.

In order to rewrite the equation (4.1) for the velocities, we define the scattering shift matrix⁷

$$M_{kj} = 2 \min(k, j). \tag{5.1}$$

For the time evolution generated by T_l , the effective velocity $v_k^{(l)}$ of amplitude- k solitons in a state with soliton densities $\{\rho_j\}$ satisfies (4.1), i.e.,

$$v_k^{(l)} = \kappa_k^{(l)} - \sum_{j=1}^{\infty} M_{kj}(v_j^{(l)} - v_k^{(l)})\rho_j. \tag{5.2}$$

In the expression above the vector $\kappa^{(l)}$ encodes the bare soliton velocities and is defined by $\kappa_k^{(l)} = \min(k, l)$ as in (4.7). In this section we will however omit the superscript (l) for all quantities, for brevity. We thus have, in a compact form

$$(1 - M\rho) * v = \kappa - M(\rho * v). \tag{5.3}$$

Next we know that the hole density is given by (3.9):

$$\sigma = 1 - M\rho \tag{5.4}$$

with 1 denoting the vector $(1, 1, \dots)$. We can define so-called filling fractions y_i by $y_i = \rho_i/\sigma_i$. They correspond to Y_i^{-1} in (3.11), and the vector y satisfies

$$y * \sigma = \rho. \tag{5.5}$$

The relations (5.4) and (5.5) are equivalent to (3.8) and (3.9). As we will see, the vector y plays a central role in the solution of the GHD equations.

The knowledge of y allows us to define a ‘dressing’ operation. To any vector o we associate a corresponding dressed vector o^{dr} which satisfies:

$$o^{\text{dr}} = o - M\mathbf{y}o^{\text{dr}}. \tag{5.6}$$

In practice o^{dr} can be computed from o using the inverse of the matrix $1 + M\mathbf{y}$:

$$o^{\text{dr}} = (1 + M\mathbf{y})^{-1}o. \tag{5.7}$$

In particular, (5.4) and (5.5) imply that

$$\sigma = 1 - M\mathbf{y}\sigma \tag{5.8}$$

and thus

$$\sigma = 1^{\text{dr}}. \tag{5.9}$$

Using (5.5) and (5.8) we can rewrite (5.3) as

$$(1 - M\mathbf{y}\sigma) * v = \kappa - M\mathbf{y}(\sigma * v) \tag{5.10}$$

or

$$\sigma * v = \kappa - M\mathbf{y}(\sigma * v), \tag{5.11}$$

⁷The diagonal of M does not enter (5.2), and this leads to several possible choices for the matrix M .

which means that $\sigma * v = \kappa^{\text{dr}}$ and, from (5.9)

$$1^{\text{dr}} * v = \kappa^{\text{dr}}. \tag{5.12}$$

The equation above provides a way to compute the effective velocities from the knowledge of y , using the dressing of two known vectors, 1 and κ . This gives naturally rise to a formal expansion in powers of y (but y does not need to be small). Notice that (5.8) coincides with (3.1), and (5.11) with (4.22), in a slightly disguised form.

Remark 5.1. Other choices for diagonal part of the matrix M are possible, since its diagonal does not enter (5.2). In particular we can define $n = (1 + y^{-1})^{-1}$. Then, replacing M by $\tilde{M} = M - 1$ modifies the previous expressions as follows: $M \rightarrow \tilde{M}$, $y \rightarrow n$, $\sigma \rightarrow r = \rho + \sigma$. So, (5.8) and (5.11) become:

$$r = 1 - \tilde{M}\mathbf{n}r, \tag{5.13}$$

$$r * v = \kappa - \tilde{M}\mathbf{n}(r * v), \tag{5.14}$$

And the dressing gets modified accordingly.

For any vector h , one can define a charge $q_h = \sum_k h_k \rho_k = h \cdot \rho$ which is conserved. The dressing enables to express q_h in terms of y :

$$q_h = h \cdot \rho = h^{\text{dr}} \cdot y. \tag{5.15}$$

Indeed:

$$h \cdot \rho = h \cdot \mathbf{y}1^{\text{dr}} = (1 + \mathbf{y}M)^{-1}\mathbf{y}h \cdot 1 = \mathbf{y}(1 + M\mathbf{y})^{-1}h \cdot 1 = h^{\text{dr}} \cdot y$$

The BBS is a concrete realization of a *linearly degenerate hydrodynamic system* [4, 35] (see also [24]), which we briefly describe in appendix F.

5.2. Dynamics of an inhomogeneous system

We want to consider an inhomogeneous system, with the hypothesis that it can be locally described using the above formalism, but where all densities have acquired a dependence on space ($x = i/L$, $i =$ lattice index) and time ($t = i/L$, $i =$ time step). The main assumption is that the hole current $(j_\sigma)_k$ associated to amplitude- k solitons is given by

$$(j_\sigma)_k = \sigma_k v_k \tag{5.16}$$

and we have the hole conservation equation⁸

$$\partial_t \sigma + \partial_x j_\sigma = 0. \tag{5.17}$$

Remarkably, it implies that the curves y_k constant are characteristics. Using $\sigma = (1 + M\mathbf{y})^{-1}1$, the above equation rewrites:

$$\partial_t((1 + M\mathbf{y})^{-1})(1) + \partial_x((1 + M\mathbf{y})^{-1})(\kappa) = 0. \tag{5.18}$$

⁸ σ_k can be replaced by $f_k(y_k)\sigma_k$ and j_σ by $f_k(y_k)j_\sigma$ with f_k arbitrary. In particular, taking $f_k(y_k) = y_k$, we recover the soliton conservation equation $\partial_t \rho + \partial_x(v * \rho) = 0$.

One has:

$$\partial_\alpha((1 + M\mathbf{y})^{-1}) = -\beta(\partial_\alpha\mathbf{y})(1 + M\mathbf{y})^{-1} \quad \text{with } \alpha = t \text{ or } x. \quad (5.19)$$

where β is the matrix $\beta = (1 + M\mathbf{y})^{-1}M$. Factorizing β out of (5.18) we finally get

$$\partial_t y + \mathbf{v}\partial_x y = 0, \quad (5.20)$$

which means that the y are the normal modes of the hydrodynamics [11]. We now assume that the system exhibits some ballistic scaling, so that y_k only depends on the rays $\zeta = x/t$. Then (5.20) becomes

$$(\zeta - v_k)\partial_\zeta y_k = 0. \quad (5.21)$$

The equation above means that $y_k(\zeta)$ must be constant except for possible discontinuities at wave fronts $\zeta = v_k$. Since the set of velocities is discrete in this problem, we expect the state of the system to be piecewise constant in the variable ζ . This will be confirmed by the calculations presented in the following paragraphs, as well as by the simulations.

5.3. Current conservation and discontinuities in y

We want to show that the filling fraction of a soliton can change discontinuously across the wave front $x/t = v_k$, equal to its speed, without violating the current conservation. We show it for the following systems which are more general than (5.8) and (5.11):

$$\sigma = \alpha - M\mathbf{y}\sigma, \quad (5.22)$$

$$\sigma * v = \kappa - M\mathbf{y}(\sigma * v), \quad (5.23)$$

where α and κ are arbitrary vectors, and M an arbitrary symmetric matrix. Let y denote the filling fraction vector. The dressing is defined as earlier (5.6) and $\sigma = \rho/y = \alpha^{\text{dr}}$, $v = \kappa^{\text{dr}}/\sigma$.

Let $P = (1 + M\mathbf{y})$, and D its determinant. For o a vector, let us denote $P(o)$ the vector with components $P_i(o)$ equal to the determinants of the matrices obtained by substituting o to the i th column of P . The dressing can be expressed as: $D\sigma^{\text{dr}} = P(o)$. The y_k dependence of P is only through its k th column. With this notation,

$$v_k = \frac{\kappa_k^{\text{dr}}}{\alpha_k^{\text{dr}}} = \frac{P_k(\kappa)}{P_k(\alpha)}, \quad (5.24)$$

and as a result, the speed of the soliton k does not depend on y_k .

In the frame moving at speed v_k , the continuity of the j -soliton current takes the form

$$\sigma_j^L(v_j^L - v_k) = \sigma_j^R(v_j^R - v_k) \quad (5.25)$$

where L, R refer to the regions $x/t < v_k$ and $x/t > v_k$. To show that (5.25) holds when $y_k^L \neq y_k^R$ we need to verify that both sides do not depend on y_k .

Let us denote $P_{ij}(o, o')$ the antisymmetric tensor of the determinants of the matrices obtained by substituting o to the i th column and o' to the j th column of P . The Desnanot–Jacobi identity (also called Sylvester determinant identity) rewrites:

$$P_j(o)P_k(o') - P_k(o)P_j(o') = DP_{jk}(o, o') \quad (5.26)$$

Taking $o = \kappa$ and $o' = \alpha$ we obtain:

$$\sigma_j(v_j - v_k) = \frac{P_{jk}(\kappa, \alpha)}{P_k(\alpha)}. \tag{5.27}$$

Since neither P_{jk} nor $P_k(\alpha)$ depend on y_k , the result follows⁹.

5.4. Domain wall initial condition

Let us consider (5.21) for the time evolution of a domain-wall state with ball fugacities z_L at the left and z_R at the right of the origin. This initial state defines some filling fraction vectors y_L and y_R and we have initially $y_i(x, t = 0) = \theta(x)y_{i,R} + (1 - \theta(x))y_{i,L}$. The equation (5.21) implies that the filling fraction $y_i(x, t)$ of the solitons of size i is constant if one follows an i -soliton trajectory (at velocity $v_i(x, t)$). Since y_i only takes two values in the initial state it will stay two-valued at any later time.

Next we assume a ballistic scaling, where y_i is a function of $\zeta = x/t$. (5.21) implies that we should look for solutions where the filling fraction y_i of the soliton species i is a piece-wise constant function of $\zeta = x/t$, and taking only two possible values, $y_{i,L}$ and $y_{i,R}$. We will denote by $\zeta(k)$ the location of the k th discontinuity, where some element of the vector y jumps. In the space-time region $\zeta \rightarrow -\infty$ the system cannot be influenced by the right part, and we have $y_i(\zeta \rightarrow -\infty) = y_{i,L}$. Similarly, for $\zeta \rightarrow +\infty$ the system cannot be influenced by the left part, and we have $y_i(\zeta \rightarrow +\infty) = y_{i,R}$. We set $\zeta(k = 0) = -\infty$ and we call sector k th the interval $\zeta \in]\zeta(k), \zeta(k + 1)[$. With this convention the sector 0 is the initial left state. In a given sector each $y_i(\zeta)$ is constant and can take only two values ($y_{i,L}$ or $y_{i,R}$), and this encodes whether i -solitons originate from the left or from the right in this sector. Assuming that this information on the filling fractions is known for the sector k , one can compute the dressing matrix, the vector σ (thanks to $\sigma = 1^{\text{dr}}$ (5.9)), the soliton densities $\rho_j(k)$ and their velocities $v_j(k)$ (see section 5.1).

How to determine the locations $\zeta(k)$ of the boundaries between sectors ? First, (5.21) implies that a filling fraction y_j can be discontinuous in ζ only if ζ matches the velocity of j -solitons. In particular there exists some soliton size j such that $y_j(\zeta)$ jumps from $y_{j,L}$ to $y_{j,R}$ in $\zeta = \zeta(k + 1)$, and $\zeta(k + 1) = v_j(k)$. In a similar way, decreasing ζ toward $\zeta(k)$ shows that $\zeta(k)$ is also a soliton velocity in that sector ($\exists j'$ such that $\zeta(k) = v_{j'}(k)$). Let us assume that some solitons of size i have a velocity $v_i(k)$ satisfying $\zeta(k) < v_i(k) < \zeta(k + 1)$, and let us show that it leads to a contradiction. Indeed, kinematic considerations show that, in this sector some of these i -solitons would originate from the left ($\rightarrow y_i = y_{i,L}$), and some would originate from the right ($\rightarrow y_i = y_{i,R}$), but this is incompatible with a vector y being well defined and constant inside a sector. We thus conclude that $\zeta(k)$ and $\zeta(k + 1)$ are two consecutive speeds in the spectrum of the velocities in the sector k , the solitons with velocity $\zeta(k)$ originate from the left, and those with velocity $\zeta(k + 1)$ originate from the right. In fact we observed that in a given sector all the velocities $v_i(k)$ are increasing functions of the size i . Therefore, consecutive velocities also correspond to consecutive soliton sizes.

So, in terms of the filling fraction the solution has the following simple structure, where the step number k is a discontinuity for y_k :

⁹The same type of argument enables to show that for M given by (5.1), if $\alpha_j = \alpha_l$ and $\kappa_j = \kappa_l$ for $j \geq l$, one also has $v_j = v_l$.

$$y(\zeta < \zeta(1)) = \begin{pmatrix} y_{1,L} \\ y_{2,L} \\ y_{3,L} \\ \dots \end{pmatrix} \tag{5.28}$$

$$y(\zeta(1) < \zeta < \zeta(2)) = \begin{pmatrix} y_{1,R} \\ y_{2,L} \\ y_{3,L} \\ \dots \end{pmatrix} \tag{5.29}$$

$$y(\zeta(2) < \zeta < \zeta(3)) = \begin{pmatrix} y_{1,R} \\ y_{2,R} \\ y_{3,L} \\ \dots \end{pmatrix} \tag{5.30}$$

$$y(\zeta(k) < \zeta < \zeta(k+1)) = \begin{pmatrix} \dots \\ y_{k,R} \\ y_{k+1,L} \\ \dots \end{pmatrix} \tag{5.31}$$

$$y(\zeta(l) < \zeta) = \begin{pmatrix} y_{1,R} \\ y_{2,R} \\ y_{3,R} \\ \dots \end{pmatrix} \tag{5.32}$$

Since $y_k(\zeta)$ is discontinuous at $\zeta = \zeta(k)$, $\zeta(k)$ must coincide with the velocity $v_k(k-1)$ evaluated in the sector $k-1$. But the velocity of the i -solitons does not depend on y_i (argument given in section 5.3) and y_k is the only filling fraction which changes from sector $k-1$ and k . So the velocity of the k -solitons does not change when going from the sector $k-1$ to the sector k . In other words $\zeta(k) = v_k(k) = v_k(k-1)$.

This piecewise structure is illustrated in figure 2, where the densities $\rho_j(r, t)$ are plotted as a function $\zeta = r/t$ for $k = 1, 2$ and 3 in a case with $l = 3$. Note that above we have omitted the (l) superscript, but in general the plateaux boundaries $\zeta(k)$ depend on the capacity l of the carrier ($p_L = 0$ is a notable exception, discussed in section 5.7). For the T_l evolution, we can restrict the consideration to the l first solitons $k \leq l$ since the velocities v_k are all equal for $k \geq l$. So there are $l+1$ sectors $[-\infty, \zeta(1)], \dots, [\zeta(l), \infty]$, as anticipated in (5.28)–(5.32).

The figure 3 presents the ball density measured in a simulation for a domain-wall initial state with $p_L > 0$ and $p_R > 0$. In the same plot we have shown (dotted lines) the heights and positions of the plateaux predicted by the method described above, and the agreement with the numerical results is excellent.

5.5. Case $l = 2$

Equating the current associated to amplitude- j solitons on both sides of the transition from the plateau k and $k+1$ (which is located at $\zeta = \zeta(k+1) = v_{k+1}(k+1)$) reads:

$$\rho_j(k) [v_j(k) - \zeta(k+1)] = \rho_j(k+1) [v_j(k+1) - \zeta(k+1)]. \tag{5.33}$$

The equation above was obtained from (5.25) by replacing σ by ρ , which is legitimate thanks to the footnote⁸. In the simple case with $l = 2$ these equations can be solved directly, bypassing the use of $y(\zeta)$. Let us focus for instance on $p_L > 0$ and $p_R = 0$, as illustrated in the left panel of

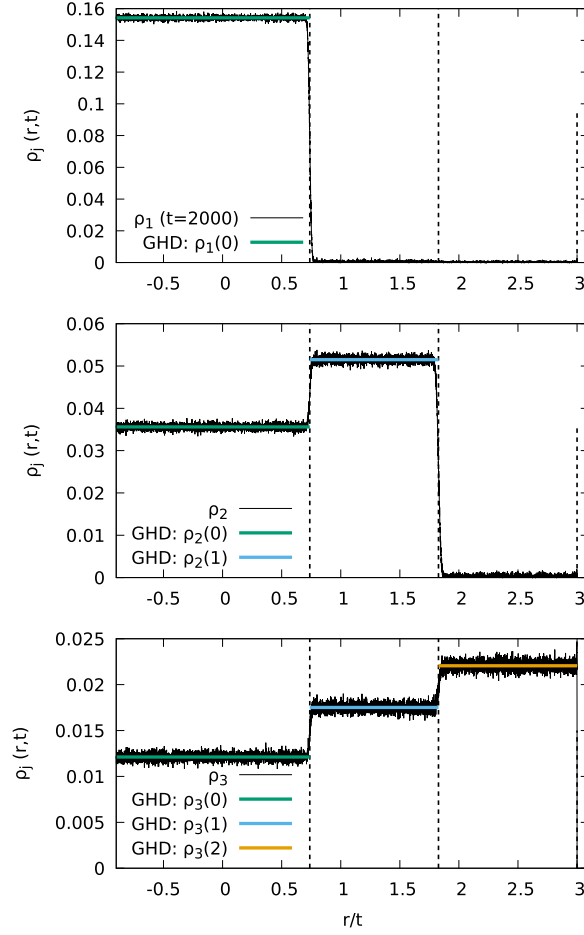


Figure 2. Soliton densities ρ_i for $i = 1$ (top panel), $i = 2$ (middle pane) and $i = 3$ (bottom). These densities are plotted as a function $\zeta = r/t$ for $l = 3$ and $t = 2000$. Here we used $N_{\text{samples}} = 2 \times 10^5$ random initial conditions with initial ball densities $p_L = 0.3$ and $p_R = 0$ (same parameters as in figure 6). One observes the disappearance of the solitons of size k when going from the plateau $k - 1$ to the plateau k , as expected from GHD. Furthermore, the densities of the various types of solitons in each plateau are in quantitative agreement with GHD (the horizontal lines represent the value $\rho_i(k)$ at the k th plateau obtained by solving the GHD equations).

figure 4. The ray space can be divided into three sectors (or plateaux). (0) $\zeta < v_1^{(2)}(0)$ where all the speeds $v_j^{(2)}(0)$ and all the densities $\rho_j(0)$ coincide with the homogeneous case. (1) $v_1^{(2)}(0) < \zeta < v_2^{(2)}(1) = 2$ where solitons $j = 1$ are absent and all the others move at speed $v_{j \geq 2}^{(2)}(1) = 2$. (2) $\zeta > 2$ is empty. Across the ray $\zeta(1) = v_1^{(2)}(0) = v_1^{(2)}(1)$, we use (5.33) with $k = 0$ to get:

$$\rho_j(0) \left[v_j^{(2)}(0) - v_1^{(2)}(0) \right] = \rho_j(1) \left[v_j^{(2)}(1) - v_1^{(2)}(0) \right]. \quad (5.34)$$

In the sector 1 all solitons with $j \geq 2$ move a speed 2 ($=l$), so the above equation gives:

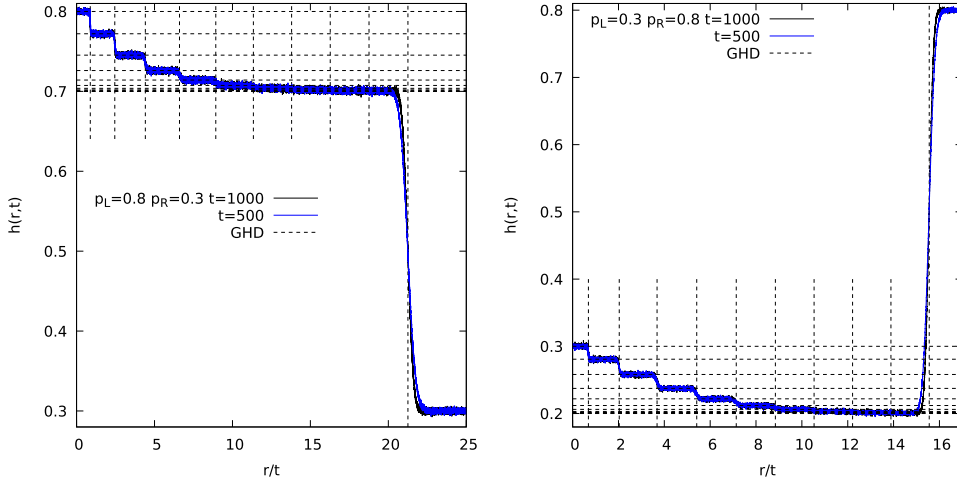


Figure 3. Left: ball density for $l = 10$, $p_L = 0.8$ and $p_R = 0.3$. The curves at $t = 1000$ (black) and $t = 500$ (blue) are practically on top of each other. Right: same for $p_L = 0.3$ and $p_R = 0.8$. Note that in the two cases the long intermediate density plateau turns out to have a ball density equal to $h = 1 - p_R$. The dotted lines are the plateau heights and positions obtained by solving numerically the GHD equations (section 5.4).

$$\rho_{j \geq 2}(1) = \rho_j(0) \frac{v_j^{(2)}(0) - v_1^{(2)}(0)}{2 - v_1^{(2)}(0)}. \tag{5.35}$$

Knowing that the speed $v_j^{(l)}(0)$ in the sector 0 (equivalent to the homogeneous state) is independent of j for $j \geq l$, we have $v_{j \geq 2}^{(2)}(0) = v_2^{(2)}(0)$ and we can write

$$\rho_{j \geq 2}(1) = \rho_j(0) \frac{v_2^{(2)}(0) - v_1^{(2)}(0)}{2 - v_1^{(2)}(0)}. \tag{5.36}$$

Together with $\rho_1(1) = 0$ the above equation gives the soliton content of the sector 1 in terms of known properties of the homogeneous state. Finally we get the ball density in that sector:

$$h(1) = \sum_{j \geq 1} j \rho_j(1) = \frac{v_2^{(2)}(0) - v_1^{(2)}(0)}{2 - v_1^{(2)}(0)} \sum_{j \geq 2} j \rho_j(0). \tag{5.37}$$

An explicit calculation of the above sum gives finally

$$h(1) = \frac{z^4 + z^3 + 2z^2}{z^4 + z^3 + 4z^2 + z + 1}, \tag{5.38}$$

in agreement with the numerical results of the left panel of figure 4. The heights and positions of the plateaux for $p_L > 0$ and $p_R = 0$ and an arbitrary value of l will be given in the next subsection (section 5.6). The reversed case ($p_L = 0$ and $p_R > 0$) is discussed in section 5.7.

5.6. Explicit plateaux solutions for $0 < p_L < \frac{1}{2}$ and $p_R = 0$

We again use the parameter z related to p_L by $p_L = \frac{z}{1+z}$ ($0 < z < 1$) and the shorthand

$$[j] = 1 - z^j \tag{5.39}$$

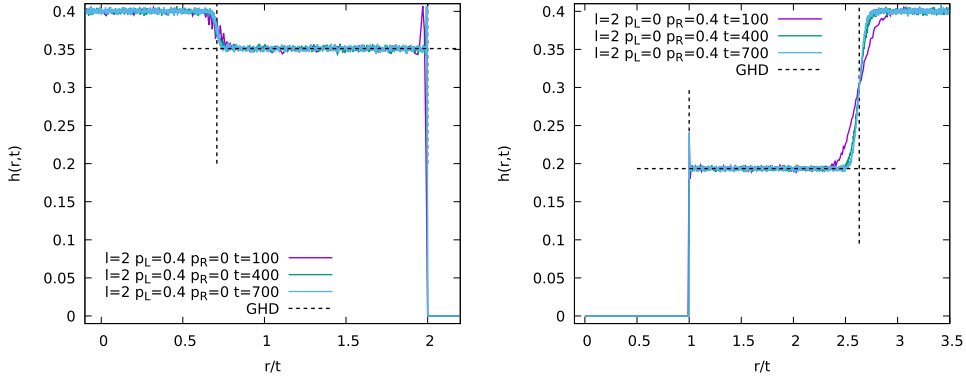


Figure 4. Left: ball density plotted as a function $\zeta = r/t$ for the carrier capacity $l = 2$ and different times. The initial ball densities: $p_L = 0.4$ and $p_R = 0$. A zoom on the density spike at $\zeta = 2$ is displayed in figure 8. The horizontal dotted line represents the GHD prediction for the ball density at the nontrivial plateau ($h(1) = 0.3511$, see (5.38) and (5.48)). The vertical dotted lines represent the GHD prediction for the end points of this plateau ($\zeta^{(2)}(1) = 0.7085$ and $\zeta^{(2)}(2) = 2$, see (5.50)). Right: same, but with $p_L = 0$ and $p_R = 0.4$. In that case the density spike is at $\zeta = 1$ and we have $h(1) = 0.1935$ (from (5.57)), $\zeta(1) = 1$ and $\zeta(l) = 2.6316$ (from (5.58)) as solutions of the GHD equations, in good agreement with the simulations.

when the formula is bulky. Let us number the plateaux as $k = 0, 1, 2, \dots$ from the left to the right, where the leftmost 0th one is of height p_L . We employ the GHD equations in the convention of remark 5.1. Thus we use the velocity of the j -soliton $v_j(k)$, the total density $r_j(k) = \rho_j(k) + \sigma_j(k)$ and the occupancy $n_j(k) = \frac{\rho_j(k)}{\rho_j(k) + \sigma_j(k)}$ which satisfy $\rho_j(k) = n_j(k)r_j(k)$ for the k th plateau. The $(n_j(k))_{j \geq 1}$ for the k th plateau is given by

$$n_j(k) = \theta(j > k) \frac{z^j(1-z)^2}{(1-z^{j+1})^2}. \tag{5.40}$$

See (2.8) for the definition of θ . The other factor is derived as $n_j = (1 + Y_j)^{-1} = (1 + Q_{i-1}Q_{i+1})^{-1} = (Q_i)^{-2}$ by using (3.11), (3.18) and (3.19) with $a = z$. For the time evolution T_∞ , the GHD equations read as

$$r_i(k) = 1 - \sum_{j=1}^{\infty} \tilde{M}_{ij} n_j(k) r_j(k), \tag{5.41}$$

$$r_i(k) v_i(k) = i - \sum_{j=1}^{\infty} \tilde{M}_{ij} n_j(k) r_j(k) v_j(k), \tag{5.42}$$

where $\tilde{M}_{ij} = (M - 1)_{ij} = 2 \min(i, j) - \delta_{ij}$ according to (5.1) and remark 5.1.

For the time evolution T_l , (5.41) remains the same, whereas the first term i on the RHS of (5.42) is replaced by $\min(l, i)$ (see also (5.2)). The solution of (5.41) is given by

$$r_j(k) = \frac{[2k + 3] + (2k + 1 - 2j)[1]z^{k+1}}{[2k + 3] + (2k + 1)[1]z^{k+1}} \quad (1 \leq j \leq k), \tag{5.43}$$

$$= \frac{[k + 1][k + 2][2j + 2]}{[j][j + 2]([2k + 3] + (2k + 1)[1]z^{k+1})} \quad (j > k). \tag{5.44}$$

The solution to (5.42) is given by

$$v_j(k) = \frac{j[k+1][k+2]}{(1+z^{k+1})[k+2]+2(k-j)[1]z^{k+1}} \quad (1 \leq j \leq k), \quad (5.45)$$

$$= \frac{\Gamma_j(k)}{(1+z^{j+1})[k+1][k+2]} \quad (j > k), \quad (5.46)$$

where $\Gamma_j(k)$ is defined by

$$\begin{aligned} \Gamma_j(k) &= 2k^2 z^{k+2}[j] - 2(k+1)^2 z^{k+1}[j+2] - 2z^{2k+3}[j-2k-2] \\ &\quad - \frac{4z^{k+2}[j-k][k+1]}{[1]} + j(1+z^{j+1})([2k+3] + (1+2k)[1]z^{k+1}). \end{aligned} \quad (5.47)$$

From these results, the height $h(k)$ of the k th plateau is calculated as

$$h(k) = \sum_{j=1}^{\infty} j \rho_j(k) = \sum_{j=k+1}^{\infty} j n_j(k) r_j(k) = \frac{z^{k+1}([k+2] + k[1])}{[2k+3] + (2k+1)[1]z^{k+1}}. \quad (5.48)$$

This certainly satisfies $h(0) = \frac{z}{1+z} = p_L$. And evaluating the above height for $k = 1$ gives back (5.38).

The position $\zeta(k)$ of the boundary of the $(k-1)$ th and the k th plateaux is

$$\zeta(k) = v_k(k) = \frac{k(1-z^{k+1})}{1+z^{k+1}} \quad (5.49)$$

for $k \geq 1$. One can check from (5.45) and (5.46) that $v_k(k-1) = v_k(k) = \zeta(k)$ for $k \geq 1$, in agreement with the discussion given in section 5.4.

For T_l with finite l , the height of the k th plateau is given by $\theta(k < l)h(k)$ with $h(k)$ still given by (5.48). On the other hand, the position $\zeta(k)$ gets modified into

$$\zeta^{(l)}(k) = \frac{k(1-z^{k+1})(1+z^{l+1})}{(1+z^{k+1})(1-z^{l+1})} \quad (1 \leq k \leq l). \quad (5.50)$$

The figures 1 and 2, the left panel of figure 4, the left panel of figures 5, 6 and 7 correspond to situations $p_L > 0$ and $p_R = 0$, as discussed above. The heights of the plateaux turn out to be independent of l , but their positions depend on l . These heights and positions are in perfect agreement with the GHD results of equations (5.48) and (5.50).

5.7. Explicit plateaux solutions for $p_L = 0$ and $0 < p_R < \frac{1}{2}$

Set $p_R = \frac{z}{1+z}$. Let us number the plateaux as $k = 0, 1, 2, \dots$ from the left to the right, where the leftmost 0th one is of height 0. Then the occupation function of the k th plateau is

$$n_j(k) = \theta(j \leq k) \frac{z^j(1-z)^2}{(1-z^{j+1})^2}, \quad (5.51)$$

which is complementary to (5.40). The GHD equations are formally the same as (5.41) and (5.42) except that $n_j(k)$ is now specified as (5.51) instead of (5.40). Note that the sums in (5.41)

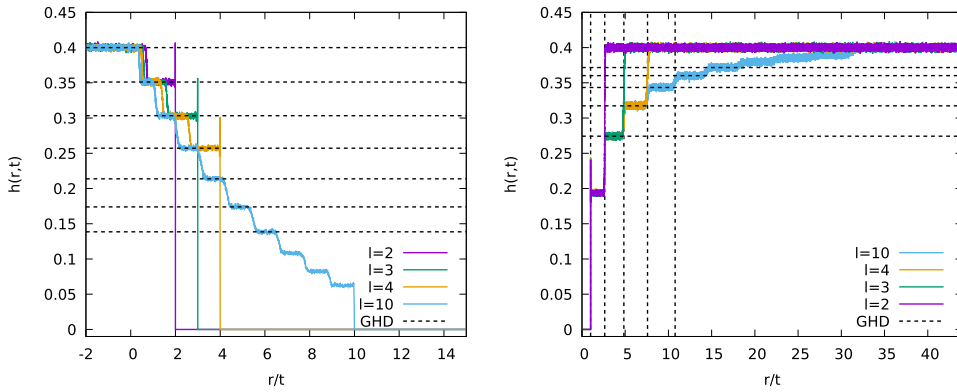


Figure 5. Left: ball density plotted as a function r/t for the carrier capacities $l = 2, 3, 4$ and 10 , at fixed $t = 500$. Initial ball densities: $p_L = 0.4$ and $p_R = 0$. The ball density is zero for $r/t > l$. One can see that the density of the first plateau ($h(1) \simeq 0.35$) is the same for $l = 2, 3, 4$ and 10 . Similarly, the second plateau has the same density for $l = 3, 4$ and 10 , etc. This fact is well reproduced in the GHD approach (section 5.6). Right: same with $p_L = 0$ and $p_R = 0.4$ (for $t = 1000$). Now we observe that not only the plateau heights, but also the plateau positions (velocities) are independent of l (vertical dotted lines), in agreement with the results of section 5.7. Note that the last plateau for $l = 10$ starts at $\zeta(10) \simeq 31.2866$, a velocity which is significantly larger than the largest bare velocity $l = 10$.

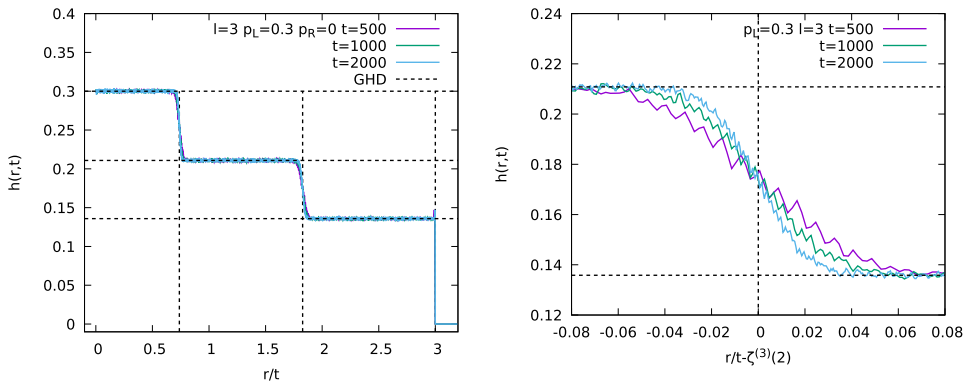


Figure 6. Left: ball density plotted as a function $\zeta = r/t$ for $l = 3$ and different times. Initial ball densities: $p_L = 0.3$ and $p_R = 0$. The horizontal dotted line represents the GHD prediction for the ball densities in each plateau (5.48) and the vertical dotted lines represent the GHD prediction for the end points of the plateaux (5.49). Here $N_{\text{samples}} = 2 \times 10^5$ and $L = 2 \times 10^5$. Right: zoom on the vicinity of the transition from the first to the second plateau at $\zeta^{(3)}(2) \simeq 1.827$ (5.50). The erratic variations reflect the statistical fluctuations (N_{samples} is large but finite). The quantitative analysis of the (diffusive) broadening of the transition is carried out in section 5.8

and (5.42) over j are reduced to the finite one over $1 \leq j \leq k$. The solution to (5.41) on $r_j(k)$ is

$$r_j(k) = \frac{[1][j+1]X_j(k)}{(1+z)[j][j+2]([2k+3] - (2k+3)[1]z^{k+1})} \quad (1 \leq j \leq k), \quad (5.52)$$

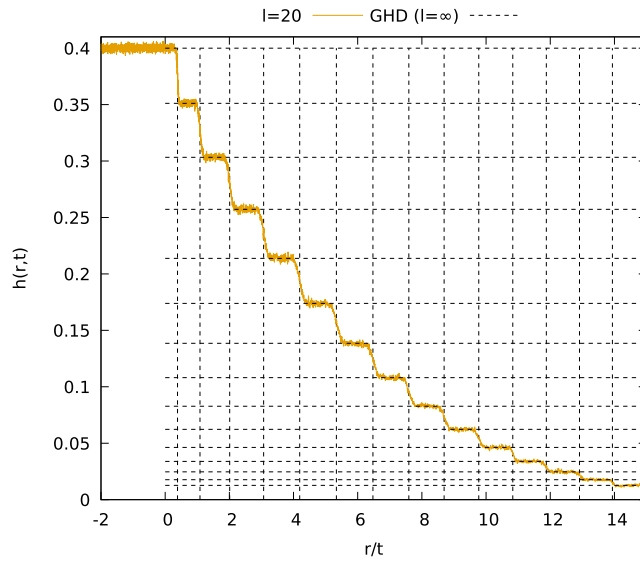


Figure 7. Ball density for the capacity $l = 20$ at fixed $t = 500$. Initial ball densities: $p_L = 0.4$ and $p_R = 0$. The dotted lines correspond to the horizontal and vertical positions of the plateaux predicted by the GHD approach in the limit $l = \infty$, see (5.48) and (5.49).

$$= \frac{[1][k+1][k+2]}{(1+z)([2k+3] - (2k+3)[1]z^{k+1})} \quad (j > k). \tag{5.53}$$

The solution to (5.42) on the velocity $v_j(k)$ is

$$v_j(k) = \frac{(1+z)[k+1][k+2](j[j+2] - (j+2)[j]z)}{[1]^2 X_j(k)} \quad (1 \leq j \leq k), \tag{5.54}$$

$$= \frac{(1+z)((2k(k+2) - j(2k+3))[1]^2 z^{k+1} - 2z[k][k+2] + j[1][2k+3])}{[1]^2 [k+1][k+2]} \quad (j > k), \tag{5.55}$$

where $X_j(k)$ in (5.52) and (5.54) is defined by

$$X_j(k) = (1+z^{j+1})[2k+3] + (2k-2j-1)[j]z^{k+2} - (2k-2j+3)[j+2]z^{k+1}. \tag{5.56}$$

From these results, the height $h(k)$ of the k th plateau is calculated as

$$h(k) = \sum_{j=1}^{\infty} j \rho_j(k) = \sum_{j=1}^k j n_j(k) r_j(k) = \frac{z([2k+2] - (k+1)[2]z^k)}{(1+z)([2k+3] - (2k+3)[1]z^{k+1})}. \tag{5.57}$$

This certainly satisfies $h(0) = 0$ and $h(\infty) = \frac{z}{1+z} = p_R$.

The position $\zeta(k)$ of the boundary of the $(k-1)$ th and the k th plateaux is

$$\zeta(k) = v_k(k) = \frac{1+z^{k+1}}{1-z^{k+1}} \left(k \frac{1+z}{1-z} - \frac{2z(1+z)(1-z^k)}{(1-z)^2(1+z^{k+1})} \right) = v_k^{(k)} \Big|_{a=z} \text{ in (D.2)}. \tag{5.58}$$

In particular one has $\zeta(1) = 1$. And here also one can check from (5.54) and (5.55) that $v_k(k - 1) = v_k(k) = \zeta(k)$ for $k \geq 1$.

It is also instructive to consider (5.57) and (5.58) in the half-filled limit $z \rightarrow 1$. There one finds

$$\lim_{z \rightarrow 1} h(k) = \frac{k}{2k + 3} \tag{5.59}$$

and

$$\lim_{z \rightarrow 1} \zeta(k) = \frac{1}{3}k(k + 2), \tag{5.60}$$

with a step position $\zeta(k)$ which turns out to grow much faster than the bare velocity k .

For T_l with finite l , the results (5.57) remains valid for $0 \leq k \leq l - 1$ and $h(l) = \frac{z}{1+z} = p_R$. The result (5.58) is valid for $1 \leq k \leq l - 1$.

The right panel of figure 4 and the right panel of figure 5 describe such situations, where $p_L = 0$ and $p_R > 0$. In such cases, the heights *and* the positions (or velocities) of the plateaux indeed appear to be independent of l , as expected from the GHD results presented above.

5.8. Transitions between plateaux and diffusive broadening of the steps

At this stage the GHD approach predicts sharp (i.e. discontinuous) steps/transitions between plateaux in the variable ζ . However, in the numerical simulations, the steps in the density curves (ball density or soliton densities) exhibit some visible widths. This can be seen, for instance, in the right panel of figure 6. A careful analysis of the time-dependence of these transition regions, as proposed in figure 9, shows that the spatial extent of these regions is $\sim \sqrt{t}$ in the variable r , corresponding to a diffusive behavior.

The finite widths of the plateau transitions can be interpreted as the fact that some solitons have traveled faster or more slowly than the mean velocity predicted by GHD. This is to be expected, as the soliton densities are fluctuating from one initial configuration to another, and these density fluctuations induce velocity fluctuations. If one assumes that the density fluctuations that a given tagged soliton ‘sees’ are uncorrelated, its mean velocity computed over a certain time will be distributed in a Gaussian way (for long enough time). This should lead to a diffusive broadening of the transitions between consecutive plateaux, as observed numerically. We stress that the dynamics is here completely deterministic, and the diffusion originates from the randomness in the initial conditions.

In the following we explain how to describe quantitatively this diffusive broadening. We will describe how to compute the shape of the density curves joining two consecutive plateaux. There is already a abundant literature on diffusive corrections to GHD [9, 10, 12, 21, 22] and the argument we propose below in the context of the BBS is close to the one given in [21].

Across the characteristic (wave front) between plateau $k - 1$ and k , the pseudoenergy ϵ_k defined by $y_k = \exp(-\epsilon_k)$ changes abruptly from $\epsilon_k(k - 1) = (\epsilon_L)_k$ to $\epsilon_k(k) = (\epsilon_R)_k$. At position r and time t , it takes the value $(\epsilon_L)_k$ or $(\epsilon_R)_k$ according to whether it is located left or right of the fluctuating wave front. In other words, its value depends if the average velocity of the wave-front position, $\bar{v}_k = (1/t) \int_0^t v_k(s) ds$, is larger or smaller than r/t .

The above wave-front velocity fluctuates due to fluctuations in the background of solitons $i \neq k$ crossing it. For a given random initial condition these background fluctuations can be described by pseudoenergy density fluctuations $\delta \bar{\epsilon}_i$. The fluctuations of \bar{v}_k , denoted by $\delta \bar{v}_k$,

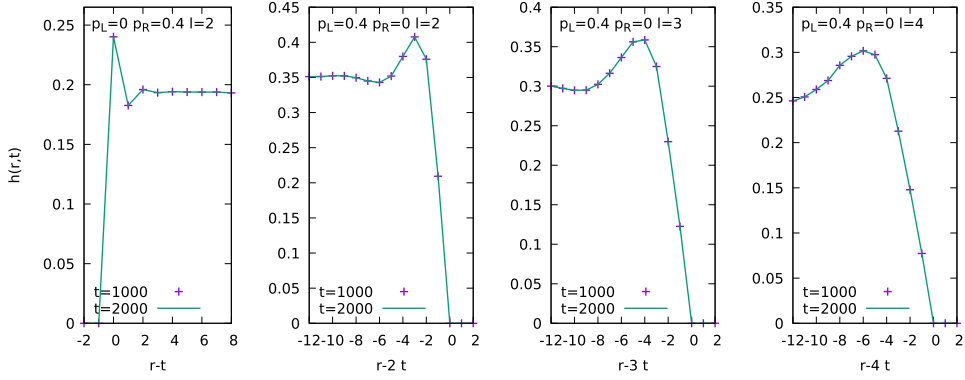


Figure 8. Ball density in the vicinity of a step to (or from) a zero-density plateau when p_L or p_R is set to zero. Contrary to the others, these steps do not broaden diffusively since there is only one species of soliton on the nontrivial side of the step. Instead, these steps show a peak (or spike) whose spatial extent is constant in time. From left to right: (i) $l = 2, p_L = 0, p_R = 0.4, \zeta = 1$ (ii) $l = 2, p_L = 0.4, p_R = 0, \zeta = 2$ (iii) $l = 3, p_L = 0.4, p_R = 0, \zeta = 3$ (iv) $l = 4, p_L = 0.4, p_R = 0, \zeta = 4$. Note that the curve at different times are superimposed.

can thus be written as

$$\delta \bar{v}_k = \sum_{i \neq k} \left(\frac{\partial v_k}{\partial \epsilon_i} \right) \delta \bar{\epsilon}_i. \tag{5.61}$$

In the above expression, the pseudoenergy density fluctuation $\delta \bar{\epsilon}_i$ is obtained by averaging the pseudoenergy over the length $t|v_i - v_k|$, which is the distance the wave front has traveled in a (moving) frame where the background of i -solitons is at rest. Assuming that the pseudoenergy fluctuations at different point in space are uncorrelated, we find that at long times $\delta \bar{v}_k$ follows a Gaussian distribution with a variance given by:

$$\langle (\delta \bar{v}_k)^2 \rangle = \sum_{i \neq k} \left(\frac{\partial v_k}{\partial \epsilon_i} \right)^2 \frac{\langle (\delta \epsilon_i)^2 \rangle}{|v_i - v_k| t}, \tag{5.62}$$

where $\langle (\delta \epsilon_i)^2 \rangle$ is the stationary (and homogeneous) i -soliton pseudoenergy variance per site. This quantity $\langle (\delta \epsilon_i)^2 \rangle$ can be obtained by a thermodynamic calculation, by expanding the free energy per site (3.7) at quadratic order in ϵ [17]. From (3.10) and (3.11), the free energy derivative is given by:

$$\frac{\partial \mathcal{F}}{\partial \epsilon_i} = \sum_{n=1}^{\infty} X_n \frac{\partial \rho_n}{\partial \epsilon_i}, \tag{5.63}$$

where $X_n = \frac{\partial \mathcal{F}}{\partial \rho_n}$ is given by the TBA equation (3.11)

$$X_n = \sum_{p=1}^{\infty} \min(n, p) \beta_p - \log(1 + e^{\epsilon^n}) + 2 \sum_{p=1}^{\infty} \min(n, p) \log(1 + e^{-\epsilon^p}) \tag{5.64}$$

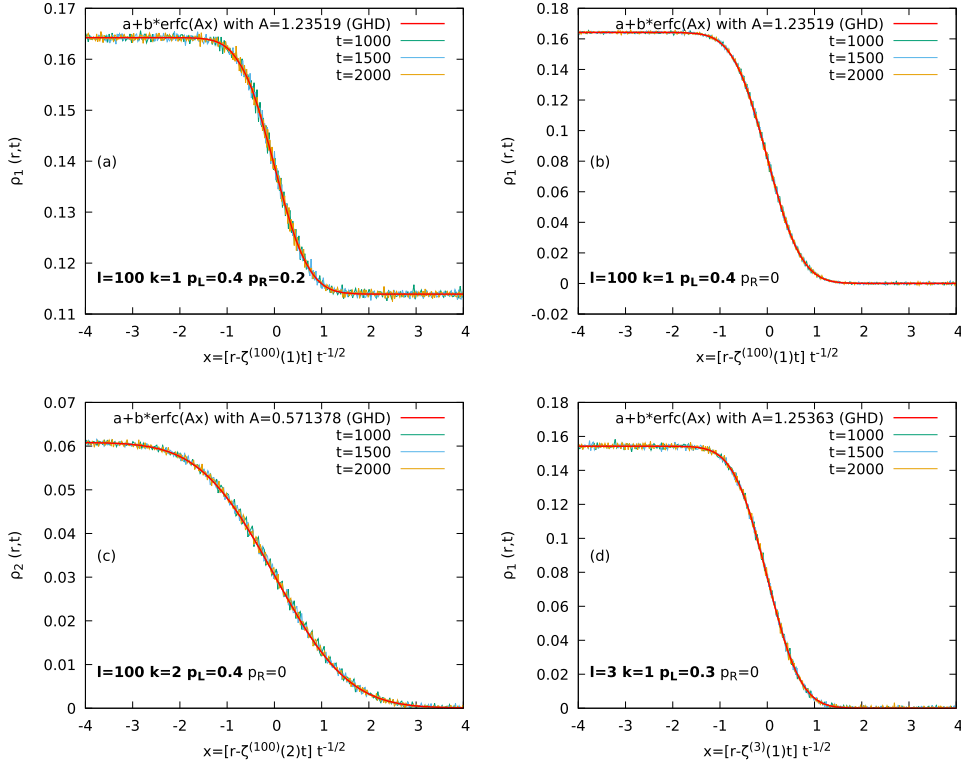


Figure 9. Zoom on the soliton density $\rho_j(r, t)$ at four different steps between plateaux. The red curves are the prediction of the diffusive corrections to GHD (5.72). In all cases the horizontal axis corresponds to $[r - \zeta^{(l)}(k)t] t^{-1/2}$ and provides a good collapse of the curves measured at different times ($t = 500, 1500$ and 2000). This shows that the scaling of the transition regions is diffusive. The high precision was achieved thanks to simulations done up to $t = 2000$ with $L = 10^6$ sites and $N_{\text{samples}} = 10^6$, corresponding to $\sim 10^{15}$ particle moves. The four panels correspond to different parameters of the model: (a) $p_L = 0.4, p_R = 0.2, l = 100$ and $k = 1$. (b) $p_L = 0.4, p_R = 0, l = 100$ and $k = 1$. (c) $p_L = 0.4, p_R = 0, l = 100$ and $k = 2$. (d) $p_L = 0.3, p_R = 0, l = 3$ and $k = 1$. The inverse width $A = 1/\sqrt{2\Sigma_k^2}$ in panel (a) was obtained by computing numerically Σ_k^2 in (5.72). In panels (b)–(d), A^2 is calculated from (5.74) with $(k, l) = (1, 100), (2, 100)$ and $(1, 3)$. The simulations and the theoretical values of $\Sigma_k^{(l)}$ agree with a $10^{-2} \sim 10^{-3}$ relative accuracy, which is the order of magnitude of the statistical fluctuations on the simulation side.

and the free energy Hessian is given by:

$$\frac{\partial^2 \mathcal{F}}{\partial \epsilon_k \partial \epsilon_p} = \sum_n \frac{\partial X_n}{\partial \epsilon_p} \frac{\partial \rho_n}{\partial \epsilon_k}, \quad (5.65)$$

where we have taken into account that it is evaluated at the minimum of the free energy, where $X_k = 0$. Using the pseudoenergies $\sigma = \rho/y = e^\epsilon \rho$, (5.4) can be rewritten as:

$$1 = (M + e^\epsilon) \rho. \quad (5.66)$$

Differentiating with respect to ρ_n we deduce:

$$\frac{\partial \epsilon_j}{\partial \rho_n} = -\sigma_j^{-1} (M + \mathbf{e}^\epsilon)_{jn} \quad (5.67)$$

and from (5.64):

$$\frac{\partial X_n}{\partial \epsilon_p} = -\frac{1}{1 + \mathbf{e}^{\epsilon_p}} (M + \mathbf{e}^\epsilon)_{pn}. \quad (5.68)$$

Substituting the inverse of (5.67) and (5.68) in (5.65) we obtain:

$$\frac{\partial^2 \mathcal{F}}{\partial \epsilon_k \partial \epsilon_p} = \delta_{kp} \frac{\sigma_k}{1 + \mathbf{e}^{\epsilon_k}}. \quad (5.69)$$

This yields diagonal pseudoenergy fluctuations¹⁰:

$$\langle \delta \epsilon_k \delta \epsilon_p \rangle = \delta_{kp} \frac{1 + \mathbf{e}^{\epsilon_k}}{\sigma_k}. \quad (5.70)$$

Now, coming back to (5.62), we need to compute the $\partial v_k / \partial \epsilon_i$ terms. These velocity derivatives can be obtained from (5.12), $v = \kappa^{\text{dr}} / 1^{\text{dr}}$, which can be written as $v = ((1 + M\mathbf{y})^{-1}\kappa) / ((1 + M\mathbf{y})^{-1}1)$. The result is:

$$\frac{\partial v_k}{\partial \epsilon_i} = \beta_{ki} \frac{\rho_i}{\sigma_k} (v_i - v_k), \quad (5.71)$$

where β is the matrix $\beta = (1 + M\mathbf{y})^{-1}M$. From the definition (5.7) of the dressing operation, β corresponds to M^{dr} .

Putting (5.62), (5.70) and (5.71), together, we obtain¹¹:

$$t \langle (\delta \bar{v}_k)^2 \rangle = \Sigma_k^2 = \sum_i \frac{\beta_{ki}^2}{\sigma_k^2} |v_k - v_i| \sigma_i y_i (1 + y_i). \quad (5.72)$$

Since we expect a Gaussian distribution of the front-velocity fluctuations in the long time limit, the above variance is essentially enough to characterize the distribution of the front position. Let us consider a local quantity, the density of j -solitons, evaluated at (r, t) for a value $\zeta = r/t$ close to the mean position $\zeta(k)$ of the step number k . For realizations such that the front has a velocity \bar{v}_k larger than ζ , the j -soliton density will be equal to its value $\rho_j(k-1)$ in the plateau $k-1$. On the other hand, for realizations such that the front has a velocity \bar{v}_k smaller than ζ , the j -soliton density will be equal to its value $\rho_j(k)$ in the plateau k . Since \bar{v}_k is distributed in a Gaussian way, the probability to be above (or below) a certain value r/t can be written simply with the complementary error function $\text{erfc}(u) = \frac{2}{\sqrt{\pi}} \int_u^\infty e^{-s^2} ds$. The Gaussian being characterized by the mean $\zeta(k)$ and the variance Σ_k^2 (5.72), the realization-averaged soliton densities in the vicinity of the step k reads:

$$\langle \rho_j(r, t) \rangle = \frac{1}{2} (\rho_j(k-1) - \rho_j(k)) \text{erfc} \left(\sqrt{\frac{t}{2}} \frac{r/t - \zeta(k)}{\Sigma_k} \right) + \rho_j(k). \quad (5.73)$$

¹⁰ This is a spectral parameter-free version of [17, equation (A.1)]. A similar result was originally given in [36] for the density correlations of the single-component boson.

¹¹ With (5.14) we obtain an equivalent expression $\Sigma_k^2 = \sum_i \frac{\tilde{\beta}_{ki}^2}{r_k^2} |v_k - v_i| r_i n_i (1 - n_i)$ with $\tilde{\beta} = (1 + \tilde{M}\mathbf{n})^{-1}\tilde{M}$.

(OCAMI) and Grants-in-Aid for Scientific Research No 16H03922, 18H01141 and 18K03452 from JSPS.

Appendix A. Transfer matrix formalism of GGE partition function of BBS

Introduce the matrices

$$V_\eta^{(l)} = (V_\eta^{(l)}(n, \tilde{n}))_{n, \tilde{n}=0}^l \in \text{Mat}(l+1, l+1) \quad (\eta \in \{0, 1\}), \quad (\text{A.1})$$

$$V_\eta^{(l)}(n, \tilde{n}) = \theta(n, \tilde{n} \text{ and } \eta \text{ fit (2.4)}) e^{-\beta_l \theta(\eta > \tilde{\eta})}, \quad (\text{A.2})$$

where θ is defined by (2.8). In (A.2), $\tilde{\eta} \in \{0, 1\}$ is also determined by the fitting diagram in (2.4). The factor $e^{-\beta_l \theta(\eta > \tilde{\eta})}$ incorporates the local Boltzmann weight from the l th energy E_l (2.7). Now consider the partition function

$$\tilde{Z}_L(\beta_1, \dots, \beta_r, \beta_\infty) = \sum_{\eta \in \{0,1\}^L} e^{-\beta_1 E_1 - \dots - \beta_r E_r - \beta_\infty E_\infty}. \quad (\text{A.3})$$

This is equal to (3.5) with the corresponding choice s of the temperatures except that the sum is not restricted by the condition mentioned under it. In the rest of this appendix, we assume L is odd¹². By the construction we have

$$\begin{aligned} \tilde{Z}_L(\beta_1, \dots, \beta_r, \beta_\infty) &= \sum_{\eta_1, \dots, \eta_L \in \{0,1\}} \text{Tr}(V_{\eta_1}^{(1)} \dots V_{\eta_L}^{(1)}) \dots \text{Tr}(V_{\eta_1}^{(r)} \dots V_{\eta_L}^{(r)}) \\ &\times e^{-\beta_\infty(\eta_1 + \dots + \eta_L)}, \end{aligned} \quad (\text{A.4})$$

where $e^{-\beta_\infty(\eta_1 + \dots + \eta_L)}$ is the Boltzmann factor for E_∞ in (2.13). We have included it separately from E_1, \dots, E_r since it can be incorporated by a simple scalar exceptionally. Define the transfer matrix V by

$$V = V_0^{(1)} \otimes \dots \otimes V_0^{(r)} + e^{-\beta_\infty} V_1^{(1)} \otimes \dots \otimes V_1^{(r)} \in \text{Mat}((r+1)!, (r+1)!). \quad (\text{A.5})$$

Then we have

$$\tilde{Z}_L(\beta_1, \dots, \beta_r, \beta_\infty) = \text{Tr}(V^L). \quad (\text{A.6})$$

This puts us in a standard situation, i.e., the free energy density in the thermodynamic limit is reduced to $-\log$ of the largest eigenvalue of the transfer matrix V . We expect that in the limit $L \rightarrow \infty$, the above $\tilde{Z}_L(\beta_1, \dots, \beta_r, \beta_\infty)$ yields the same free energy density as (3.5).

Example A.1. The transfer matrix for $\tilde{Z}_L(\beta_1, \beta_\infty)$ is

$$V = \begin{pmatrix} 1 & 0 \\ 1 & 0 \end{pmatrix} + e^{-\beta_\infty} \begin{pmatrix} 0 & e^{-\beta_1} \\ 0 & 1 \end{pmatrix}. \quad (\text{A.7})$$

By expressing β_1, β_∞ in terms of a, z according to (3.20), one finds that the largest eigenvalue of V is $\frac{1-az}{1-a}$ in agreement with the free energy result (3.21).

¹² For even L , a correction term is necessary in (A.4) to take into account of the fact that $c_l(\eta)$ satisfying (2.6) is not unique at $\sum_{i \in \mathbb{Z}_L} \eta_i = L/2$ [28, proposition 2.1].

Example A.2. The transfer matrices for $\tilde{Z}_L(\beta_1, \beta_2, \beta_\infty)$ is

$$V = \begin{pmatrix} 1 & 0 \\ 1 & 0 \end{pmatrix} \otimes \begin{pmatrix} 1 & 0 & 0 \\ 1 & 0 & 0 \\ 0 & 1 & 0 \end{pmatrix} + e^{-\beta_\infty} \begin{pmatrix} 0 & e^{-\beta_1} \\ 0 & 1 \end{pmatrix} \otimes \begin{pmatrix} 0 & e^{-\beta_2} & 0 \\ 0 & 0 & e^{-\beta_2} \\ 0 & 0 & 1 \end{pmatrix}. \tag{A.8}$$

The largest eigenvalue of this will be treated in example B.2.

Appendix B. Low temperature expansion for GGE(β_1, \dots, β_s)

Here we treat the general Y-system (3.12)–(3.14). It is written as

$$Y_i^2 = e^{\beta_i} \prod_{j=1}^s (1 + Y_j)^{A_{ij}}, \tag{B.1}$$

where the quantity A_{ij} and the related C_{ij} with its useful property are given by

$$A_{ij} = 2\delta_{ij} - C_{ij}, \quad C_{ij} = 2\theta(i = j < n) + \theta(i = j = n) - \theta(|i - j| = 1), \tag{B.2}$$

$$\sum_{j=1}^s \min(i, j) C_{jk} = \delta_{ik}, \quad \sum_{i=1}^s C_{ij} = \delta_{j,1}, \tag{B.3}$$

where θ is defined in (2.8). The matrix $(C_{ij})_{i,j=1}^s$ is the symmetrized Cartan matrix of $so(2s + 1)$. The Y-system (B.1) is transformed into another difference equation called Q-system:

$$Y_i = e^{\frac{\beta_i}{2}} \prod_{j=1}^s (\tilde{Q}_j)^{A_{ij}}, \quad (\tilde{Q}_i)^2 = e^{\frac{\beta_i}{2}} \prod_{j=1}^s (\tilde{Q}_j)^{A_{ij}} + 1. \tag{B.4}$$

Further setting

$$\tilde{Q}_i = e^{\frac{1}{2} \sum_{j=1}^s \min(i,j) \beta_j} Q_i, \quad w_i = e^{-\sum_{j=1}^s \min(i,j) \beta_j} \tag{B.5}$$

and using (B.3), the relations (B.4) are cast into

$$Y_i = w_i^{-1} \prod_{j=1}^s (Q_j)^{A_{ij}}, \quad \prod_{j=1}^s (Q_j)^{-C_{ij}} + w_i Q_i^{-2} = 1. \tag{B.6}$$

Due to $1 + Y_i^{-1} = \prod_{1 \leq j \leq s} (Q_j)^{C_{ij}}$, the free energy (3.15) is expressed as

$$\mathcal{F} = - \sum_{i,j=1}^s C_{ij} \log Q_j = - \log Q_1. \tag{B.7}$$

The latter relation in (B.6) exactly fits [26, equation (2.5)] with $D_{ij} = -C_{ij}$ and $G_{ij} = -2\delta_{ij}$. Therefore we have the power series formulas [26, equation (2.17)] and [26, equation (2.38)]. In the present setting they read as

$$Q_1^{\mu_1} \dots Q_s^{\mu_s} = \sum_{(m_1, \dots, m_s) \in (\mathbb{Z}_{\geq 0})^s} w_1^{m_1} \dots w_s^{m_s} \left(\prod_{j \in H} \frac{(q_j + 1)_{m_j - 1}}{m_j!} \right) \det (F_{jk})_{j,k \in H}, \tag{B.8}$$

$$\log Q_1 = \sum_{(m_1, \dots, m_s) \in (\mathbb{Z}_{\geq 0})^s} w_1^{m_1} \cdots w_s^{m_s} \left(\prod_{j \in H} \frac{(\bar{q}_j + 1)_{m_j - 1}}{m_j!} \right) \times \sum_{r \in H} \det(\bar{F}_{jk})_{j,k \in H \setminus \{r\}}, \tag{B.9}$$

$$q_j = \sum_{k=1}^s \min(j, k)(\mu_k - 2m_k), \quad F_{jk} = \delta_{jk}q_j + 2 \min(j, k)m_k, \tag{B.10}$$

$$\bar{q}_j = q_j|_{\mu_1 = \dots = \mu_s = 0}, \quad \bar{F}_{jk} = F_{jk}|_{\mu_1 = \dots = \mu_s = 0}, \tag{B.11}$$

$$H = \{1 \leq i \leq s \mid m_i > 0\}, \quad (x)_n = x(x+1) \cdots (x+n-1) \quad (n \in \mathbb{Z}_{\geq 0}). \tag{B.12}$$

In (B.8), the powers $\mu_1, \dots, \mu_s \in \mathbb{C}$ are arbitrary¹³, and (B.9) is deduced by differentiating (B.8) with respect to μ_1 . These formulas are outcome of the theory of *generalized Q-systems*. It is the most systematic synthesis of numerous preceding results on the constant TBA equations for XXX, XXZ type spin chains and the Sutherland-Wu equations for ideal gas with Haldane statistics. See for example [26, section 2.4] for a historical account.

From (3.5)–(3.8), (B.5) and (B.7) one can derive the energy density as

$$\varepsilon_i = \frac{\partial \mathcal{F}}{\partial \beta_i} = - \sum_{j=1}^s \min(i, j) w_j \frac{\partial \mathcal{F}}{\partial w_j} = \sum_{j=1}^s \min(i, j) w_j \frac{\partial \log Q_1}{\partial w_j}. \tag{B.13}$$

Comparing (B.13) with the left relation in (3.9) we get the density of *i*-solitons:

$$\rho_i = w_i \frac{\partial \log Q_1}{\partial w_i}. \tag{B.14}$$

Substituting (B.9) into (B.14) we obtain

$$\rho_i = \sum_{(m_1, \dots, m_s) \in (\mathbb{Z}_{\geq 0})^s} m_i w_1^{m_1} \cdots w_s^{m_s} \left(\prod_{j \in H} \frac{(\bar{q}_j + 1)_{m_j - 1}}{m_j!} \right) \times \sum_{r \in H} \det(\bar{F}_{jk})_{j,k \in H \setminus \{r\}}. \tag{B.15}$$

In view of $w_1^{m_1} \cdots w_s^{m_s} = e^{-\sum_{1 \leq j, k \leq s} \min(j, k) \beta_j m_k}$, the series (B.8), (B.9) and (B.15) are low-temperature expansions. They have a finite convergence radius mentioned after [26, equation (2.15)]. To investigate the behavior around them is beyond the scope of this paper.

Example B.1. For $s = 2$, the lower order terms $w_1^i w_2^j$ with $i, j \leq 2$ read as follows:

$$Q_1 = 1 + w_1 - w_1^2 + w_2 - 3w_1w_2 + 10w_1^2w_2 - 3w_2^2 + 20w_1w_2^2 - 105w_1^2w_2^2 + \cdots, \tag{B.16}$$

$$Q_2 = 1 + w_1 - w_1^2 + 2w_2 - 4w_1w_2 + 12w_1^2w_2 - 5w_2^2 + 28w_1w_2^2 - 135w_1^2w_2^2 + \cdots, \tag{B.17}$$

¹³ Q_i 's are power series in w_1, \dots, w_s with a unit constant term for which their complex power is unambiguously defined.

$$w_1 Y_1 = 1 + w_1 - w_1^2 + 2w_2 - 4w_1 w_2 + 12w_1^2 w_2 - 5w_2^2 + 28w_1 w_2^2 - 135w_1^2 w_2^2 + \dots, \tag{B.18}$$

$$w_2 Y_2 = 1 + 2w_1 - w_1^2 + 3w_2 - 4w_1 w_2 + 12w_1^2 w_2 - 6w_2^2 + 30w_1 w_2^2 - 140w_1^2 w_2^2 + \dots, \tag{B.19}$$

$$\rho_1 = w_1 - 3w_1^2 - 4w_1 w_2 + 30w_1^2 w_2 + 27w_1 w_2^2 - 308w_1^2 w_2^2 + \dots, \tag{B.20}$$

$$\rho_2 = w_2 - 4w_1 w_2 + 15w_1^2 w_2 - 7w_2^2 + 54w_1 w_2^2 - 308w_1^2 w_2^2 + \dots, \tag{B.21}$$

$$\varepsilon_1 = w_1 - 3w_1^2 + w_2 - 8w_1 w_2 + 45w_1^2 w_2 - 7w_2^2 + 81w_1 w_2^2 - 616w_1^2 w_2^2 + \dots, \tag{B.22}$$

$$\varepsilon_2 = w_1 - 3w_1^2 + 2w_2 - 12w_1 w_2 + 60w_1^2 w_2 - 14w_2^2 + 135w_1 w_2^2 - 924w_1^2 w_2^2 + \dots. \tag{B.23}$$

The results (A.5), (A.6) and (B.7) indicate

$$Q_1 \text{ for GGE}(\beta_1, \dots, \beta_r, 0, \dots, 0, \beta_s) \xrightarrow{s \rightarrow \infty} \text{Largest eigenvalue of } V \text{ in (A.5)}, \tag{B.24}$$

where the power series expansion of the LHS is obtained by specializing (B.8) to $\mu_k = \delta_{k,1}$.

Example B.2. The power series (B.8) for Q_1 for GGE($\beta_1, \beta_2, 0, \dots, 0, \beta_s$) converges as s gets large. In terms of the variables $z_j = e^{-\beta_j}$ ($j = 1, 2, \infty$), the lower order part of the limit is

$$Q_1 = 1 + z_1 z_2 z_\infty + z_1 z_2^2 z_\infty^2 - z_1^2 z_2^2 z_\infty^2 + z_1 z_2^2 z_\infty^3 - 3z_1^2 z_2^3 z_\infty^3 + 2z_1^3 z_2^3 z_\infty^3 \tag{B.25}$$

$$+ z_1 z_2^2 z_\infty^4 - 3z_1^2 z_2^3 z_\infty^4 - 3z_1^2 z_2^4 z_\infty^4 + 10z_1^3 z_2^4 z_\infty^4 - 5z_1^4 z_2^4 z_\infty^4 + \dots \tag{B.26}$$

up to the terms $z_1^i z_2^j z_\infty^k$ with $\min(i, j, k) \geq 1$. One can check that this indeed gives the largest eigenvalue of V in (A.8) confirming (B.24). For instance when $(z_1, z_2, z_\infty) = (0.4, 0.3, 0.2)$, they take the value 1.02511....

Appendix C. Proof of (4.14)

We illustrate the proof partly along the 4×4 example

$$\begin{aligned} & \begin{pmatrix} p_1 + 2m_1 & 2m_2 & 2m_3 & 2m_4 \\ 2m_1 & p_2 + 4m_2 & 4m_3 & 4m_4 \\ 2m_1 & 4m_2 & p_3 + 6m_3 & 6m_4 \\ 2m_1 & 4m_2 & 6m_3 & p_4 + 8m_4 \end{pmatrix} \begin{pmatrix} x_1 & x_1 & x_1 & x_1 \\ x_1 & x_2 & x_2 & x_2 \\ x_1 & x_2 & x_3 & x_3 \\ x_1 & x_2 & x_3 & x_4 \end{pmatrix} \\ &= -2 \begin{pmatrix} p_1^{-1} & p_2^{-1} & p_3^{-1} & p_4^{-1} \\ p_1^{-1} & 2p_2^{-1} & 2p_3^{-1} & 2p_4^{-1} \\ p_1^{-1} & 2p_2^{-1} & 3p_3^{-1} & 3p_4^{-1} \\ p_1^{-1} & 2p_2^{-1} & 3p_3^{-1} & 4p_4^{-1} \end{pmatrix}. \tag{C.1} \end{aligned}$$

From each row subtract the adjacent upper row starting from the bottom. The result reads

$$\begin{pmatrix} p_1 + 2m_1 & 2m_2 & 2m_3 & 2m_4 \\ -p_1 & p_2 + 2m_2 & 2m_3 & 2m_4 \\ 0 & -p_2 & p_3 + 2m_3 & 2m_4 \\ 0 & 0 & -p_3 & p_4 + 2m_4 \end{pmatrix} \begin{pmatrix} x_1 & x_1 & x_1 & x_1 \\ x_1 & x_2 & x_2 & x_2 \\ x_1 & x_2 & x_3 & x_3 \\ x_1 & x_2 & x_3 & x_4 \end{pmatrix} \\ = -2 \begin{pmatrix} p_1^{-1} & p_2^{-1} & p_3^{-1} & p_4^{-1} \\ 0 & p_2^{-1} & p_3^{-1} & p_4^{-1} \\ 0 & 0 & p_3^{-1} & p_4^{-1} \\ 0 & 0 & 0 & p_4^{-1} \end{pmatrix}. \tag{C.2}$$

From $p_i = L - 2\sum_{j=1}^4 \min(i, j)m_j$, one has the relations

$$\begin{aligned} p_1 + 2m_1 + 2m_2 + 2m_3 + 2m_4 &= p_0, & p_2 + 2m_2 + 2m_3 + 2m_4 &= p_1, \\ p_3 + 2m_3 + 2m_4 &= p_2, & p_4 + 2m_4 &= p_3, \end{aligned} \tag{C.3}$$

where $p_0 = L$. Thus taking the matrix product in (C.2) leads to the equation of the form

$$\begin{pmatrix} p_0x_1 & s_{12} & s_{13} & s_{14} \\ 0 & -p_1x_1 + p_1x_2 & s_{23} & s_{24} \\ 0 & 0 & -p_2x_2 + p_2x_3 & s_{34} \\ 0 & 0 & 0 & -p_3x_3 + p_3x_4 \end{pmatrix} \\ = -2 \begin{pmatrix} p_1^{-1} & p_2^{-1} & p_3^{-1} & p_4^{-1} \\ 0 & p_2^{-1} & p_3^{-1} & p_4^{-1} \\ 0 & 0 & p_3^{-1} & p_4^{-1} \\ 0 & 0 & 0 & p_4^{-1} \end{pmatrix} \tag{C.4}$$

for s_{ij} which will be given explicitly later. Thus the lower triangular part of the matrix equation is automatically satisfied. The diagonal part compels (4.14), i.e.,

$$x_k = -2 \sum_{j=1}^k \frac{1}{p_{j-1}p_j} \tag{C.5}$$

as a *necessary* condition. For sufficiency, one needs to further verify that (C.5) also guarantees the equalities

$$s_{ij} = -\frac{2}{p_j} \quad (i < j). \tag{C.6}$$

Let us write down the element s_{ij} for the general size $g \times g$ case. By imagining the equation (C.2) for such a situation we have

$$\begin{aligned} s_{ij} &= -p_{i-1}x_{i-1} + (p_i + 2m_i)x_i + 2(m_{i+1}x_{i+1} + \dots + m_{j-1}x_{j-1}) \\ &\quad + 2(m_j + \dots + m_g)x_j, \end{aligned} \tag{C.7}$$

where $1 \leq i < j \leq g$ and $x_0 := 0$. From $p_i = L - 2\sum_{j=1}^g \min(i, j)m_j$, one has

$$2m_k = p_{k-1} - 2p_k + p_{k+1} \quad (1 \leq k < g), \quad 2m_g = p_{g-1} - p_g. \tag{C.8}$$

Substitution of them into (C.7) gives

$$\begin{aligned}
 s_{ij} &= -p_{i-1}x_{i-1} + (p_{i-1} - p_i + p_{i+1})x_i \\
 &\quad + \sum_{i+1 \leq k \leq j-1} (p_{k-1} - 2p_k + p_{k+1})x_k + (p_{j-1} - p_j)x_j \\
 &= p_{i-1}(x_i - x_{i-1}) + p_i(x_{i+1} - x_i) \\
 &\quad + \sum_{i+1 \leq k \leq j-1} p_k(x_{k-1} - 2x_k + x_{k+1}) + p_j(x_{j-1} - x_j).
 \end{aligned}
 \tag{C.9}$$

Now that x_k dependence enters only through the difference

$$x_k - x_{k-1} = \frac{-2}{p_{k-1}p_k}
 \tag{C.10}$$

implied by (C.5), the quantity (C.9) can be expressed entirely by p_0, \dots, p_g . After many cancellations, one finds that the result exactly yields $-\frac{2}{p_j}$, completing a proof of (C.6).

Appendix D. Current in GGE(β_1, β_∞)

The general result (4.2) and (4.19) on the current and the effective speed can be evaluated explicitly in the GGE(β_1, β_∞) treated in section 3.4. In fact from (3.25) we have

$$\frac{1}{\sigma_{j-1}\sigma_j} = \frac{(1+a)^2}{(1-a)^2} + \frac{2(1+a)^2(1+z)}{(1-a)^2(1-z)} \left(\frac{1}{1+az^{j-1}} - \frac{1}{1+az^j} \right).
 \tag{D.1}$$

Thus the sum (4.19) can be taken, yielding the effective speed:

$$v_k^{(l)} = \frac{1+az^l}{1-az^l} v_{\min(k,l)}, \quad v_k = \frac{1+a}{1-a} k - \frac{2a(1+z)(1-z^k)}{(1-a)(1-z)(1+az^k)}.
 \tag{D.2}$$

Further substituting this and (3.26) into (4.2), we obtain, after some calculation, the stationary current:

$$J^{(l)} = \frac{a(1+z)}{(1+a)(1-z)} \left(1 - \frac{(1-a)z^l}{1-az^l} \right) - \frac{laz^l}{1-az^l}.
 \tag{D.3}$$

From (3.20), one deduces some typical behavior as

$$J^{(l)} = \frac{z(1-z^l - lz^l(1-z))}{(1-z)(1-z^{l+1})} + O(\beta_1) \quad (\beta_1 \rightarrow 0), \tag{D.4}$$

$$= \frac{z((1+z)(1-z^l) - lz^l(1-z))}{(1-z)^3} e^{-\beta_1} + O(e^{-2\beta_1}) \quad (\beta_1 \rightarrow \infty), \tag{D.5}$$

$$= \frac{l}{2} - \frac{l(-1 + 3y^{-1} + 3ly^{-1/2} + l^2)\beta_\infty}{12(y^{-1/2} + l)} + O(\beta_\infty^3) \quad (\beta_\infty \rightarrow 0), \tag{D.6}$$

$$= e^{-\beta_1 - \beta_\infty} + O(e^{-2\beta_\infty}) \quad (\beta_\infty \rightarrow \infty), \tag{D.7}$$

where y and z are defined in (E.3).

Appendix E. Alternative derivation of $J^{(l)}$ in $GGE(\beta_1, \beta_\infty)$

Let us rederive the current (D.3) by an independent method as a consistency check. Consider the concatenation of two vertices from (2.4) which forms a segment in the diagram for the time evolution T_l in (2.5) as

$$\begin{array}{ccc}
 \alpha & & \beta \\
 | & & | \\
 n \xrightarrow{\quad} & m & \xrightarrow{\quad} \\
 | & & | \\
 \downarrow & & \downarrow
 \end{array}
 \quad n, m \in \{0, 1, \dots, l\}, \quad \alpha, \beta \in \{0, 1\}.
 \tag{E.1}$$

Introduce the local transfer matrix T generating the Boltzmann weight of this configuration in $GGE(\beta_1, \beta_\infty)$ as

$$T|n, \alpha\rangle = \sum_{m, \beta} y^{\theta(\alpha < \beta)} z^\beta |m, \beta\rangle,
 \tag{E.2}$$

where the parameters y and z are specified by

$$y = e^{-\beta_1} = \left(\frac{z^{\frac{1}{2}} - z^{-\frac{1}{2}}}{a^{\frac{1}{2}} - a^{-\frac{1}{2}}} \right)^2, \quad z = e^{-\beta_\infty}
 \tag{E.3}$$

according to (3.20), and the local forms of the energies E_1 (2.10) and E_∞ (2.13) have been taken into account. Explicitly (E.2) reads as

$$T|n, 0\rangle = |n - 1, 0\rangle + yz|n - 1, 1\rangle \quad (1 \leq n \leq l),
 \tag{E.4}$$

$$T|0, 0\rangle = |0, 0\rangle + yz|0, 1\rangle,
 \tag{E.5}$$

$$T|n, 1\rangle = |n + 1, 0\rangle + z|n + 1, 1\rangle \quad (0 \leq n \leq l - 1),
 \tag{E.6}$$

$$T|l, 1\rangle = |l, 0\rangle + z|l, 1\rangle.
 \tag{E.7}$$

The action on the dual basis is defined by postulating $\langle n, \alpha|T|n', \alpha'\rangle = \langle n, \alpha|(T|n', \alpha'\rangle)$ and $\langle n, \alpha|n', \alpha'\rangle = \delta_{n,n'}\delta_{\alpha,\alpha'}$. Explicitly they read

$$\langle n, 0|T = \langle n + 1, 0| + \langle n - 1, 1| \quad (1 \leq n \leq l - 1),
 \tag{E.8}$$

$$\langle 0, 0|T = \langle 0, 0| + \langle 1, 0|,
 \tag{E.9}$$

$$\langle l, 0|T = \langle l, 1| + \langle l - 1, 1|,
 \tag{E.10}$$

$$\langle n, 1|T = yz\langle n + 1, 0| + z\langle n - 1, 1| \quad (1 \leq n \leq l - 1),
 \tag{E.11}$$

$$\langle 0, 1|T = yz\langle 1, 0| + yz\langle 0, 0|,
 \tag{E.12}$$

$$\langle l, 1|T = z\langle l - 1, 1| + z\langle l, 1|.
 \tag{E.13}$$

We stay in the regime $0 < a \leq z < 1$ as mentioned after (3.20). Then the left and right Perron-Frobenius eigenvectors have the eigenvalue $\frac{1-az}{1-a}$, and they are given by

$$|\psi\rangle = \frac{z(1-a)}{a(1-z)}|0, 0\rangle + \sum_{n=1}^l z^n |n, 0\rangle + \frac{z(1-z)}{1-a} \sum_{n=0}^{l-1} z^n |n, 1\rangle + z^{l+1}|l, 1\rangle,
 \tag{E.14}$$

$$\langle \bar{\psi}| = \sum_{n=0}^l \langle n, 0| + \frac{1-a}{1-z} \sum_{n=0}^l \langle n, 1|.
 \tag{E.15}$$

By writing them as $|\psi\rangle = \sum_{n,\alpha} \psi_{n,\alpha} |n, \alpha\rangle$ and $\langle \bar{\psi}| = \sum_{n,\alpha} \bar{\psi}_{n,\alpha} \langle n, \alpha|$, the probability $\mathbb{P}(n, \alpha)$ of having the (n, α) part of the configuration in (E.1) is

$$\mathbb{P}(n, \alpha) = \frac{\bar{\psi}_{n,\alpha} \psi_{n,\alpha}}{\sum_{n,\alpha} \bar{\psi}_{n,\alpha} \psi_{n,\alpha}}. \tag{E.16}$$

A direct calculation of this gives

$$\mathbb{P}(0, 0) = \frac{1 - a}{(1 + a)(1 - az^l)}, \quad \mathbb{P}(n, 0) = \frac{a(1 - z)z^{n-1}}{(1 + a)(1 - az^l)} \quad (1 \leq n \leq l), \tag{E.17}$$

$$\mathbb{P}(l, 1) = \frac{a(1 - a)z^l}{(1 + a)(1 - az^l)}, \quad \mathbb{P}(n, 1) = \frac{a(1 - z)z^n}{(1 + a)(1 - az^l)} \quad (0 \leq n \leq l - 1). \tag{E.18}$$

The probability of the capacity l carrier for holding n balls is

$$\mathbb{P}(n) = \mathbb{P}(n, 0) + \mathbb{P}(n, 1) = \begin{cases} \frac{1 - az}{(1 + a)(1 - az^l)} & (n = 0), \\ \frac{az^{n-1}(1 - z^2)}{(1 + a)(1 - az^l)} & (1 \leq n \leq l - 1), \\ \frac{az^{l-1}(1 - az)}{(1 + a)(1 - az^l)} & (n = l). \end{cases} \tag{E.19}$$

When $l \rightarrow \infty$ this result agrees with [6, lemma 3.15] by identifying the parameter p_0, p_1 therein as $p_0 = \frac{a(1-z)}{1-az}, p_1 = \frac{z(1-a)}{1-az}$. Now it is elementary to calculate the expectation value of the number of balls in the carrier as

$$\sum_{n=1}^l n\mathbb{P}(n) = \frac{a(1+z)}{(1+a)(1-z)} \left(1 - \frac{(1-a)z^l}{1-az^l} \right) - \frac{laz^l}{1-az^l}. \tag{E.20}$$

This reproduces the current (D.3).

Appendix F. Linearly degenerate hydrodynamic type systems

A junction point between GHD and linearly degenerate hydrodynamic type systems [4, 24, 35] can be constructed through the current conservation (5.17):

$$\partial_t \sigma + \partial_x(\sigma v) = 0 \tag{F.1}$$

together with the characteristic equation (5.20):

$$\partial_t y + \mathbf{v} \partial_x y = 0. \tag{F.2}$$

We now take into account that the densities σ and the velocities v are functions of the vector y , and this vector y is a function of x and t . We can thus write $\partial_t \sigma_i = \sum_p \partial_t(y_p) \partial_p \sigma_i$, where ∂_p means $\partial_p = \frac{\partial}{\partial y_p}$. Similarly, $\partial_x(\sigma_i v_i) = \sum_p \partial_x(y_p) [v_i \partial_p \sigma_i + \sigma_i \partial_p v_i]$. Combined with $\partial_t(y_p) + v_p \partial_x(y_p) = 0$, (F.1) becomes:

$$\sum_p \left\{ -v_p \partial_x(y_p) \partial_p \sigma_i + \partial_x(y_p) [v_i \partial_p \sigma_i + \sigma_i \partial_p v_i] \right\} = 0. \tag{F.3}$$

Since this relation should be verified for any vector $\partial_x y$ (one can choose arbitrarily the initial condition), we have

$$\forall i, p \quad v_p \partial_p \sigma_i = v_i \partial_p \sigma_i + \sigma_i \partial_p v_i, \tag{F.4}$$

or, equivalently:

$$\partial_p \log(\sigma_i) = \frac{\partial_p v_i}{v_p - v_i}. \tag{F.5}$$

In particular, setting $p = i$, we find that v_i does not depend on y_i :

$$\partial_i v_i = 0 \quad (\text{no summation on } i). \tag{F.6}$$

Conversely, we can use the characteristic equation (F.2) as a starting point and require the integrability conditions:

$$\partial_k \left(\frac{\partial_p v_i}{v_p - v_i} \right) = \partial_p \left(\frac{\partial_k v_i}{v_k - v_i} \right), \quad p \neq k \neq i, \tag{F.7}$$

called ‘semi-Hamiltonian’ property, together with (F.6) called ‘linear degeneracy’. The densities σ_k defining the conserved currents (F.1) are then obtained by integrating (F.7).

In the BBS case, the y dependence of the velocities follows from the equation (5.12):

$$v = \kappa^{\text{dr}} / 1^{\text{dr}}. \tag{F.8}$$

We know from the commutation of the transfer matrices $T_t, T_{t'}$ that the flows associated to two different sets of bare velocities $\kappa^{(t)}$ and $\kappa^{(t')}$ commute. One can verify this property directly within this formalism for an arbitrary pair κ, κ' of vectors, by evaluating $\frac{d}{dt} \frac{dy_i}{dt'} - \frac{d}{dt'} \frac{dy_i}{dt}$.¹⁴ A direct computation using (F.2) shows it is equal to

$$\frac{d}{dt} \frac{dy_i}{dt'} - \frac{d}{dt'} \frac{dy_i}{dt} = \sum_{p \neq i} (v'_p - v_i) (v_p - v_i) \left[\frac{\partial_p v'_i}{v'_p - v'_i} - \frac{\partial_p v_i}{v_p - v_i} \right] \partial_x y_p \partial_x y_i. \tag{F.9}$$

The term in brackets turns out to vanish due to (F.5) and to the fact that $\sigma = 1^{\text{dr}}$ does not depend on the bare velocities (κ or κ'). We thus get $\frac{d}{dt} \frac{dy_i}{dt'} = \frac{d}{dt'} \frac{dy_i}{dt}$.

ORCID iDs

Atsuo Kuniba  <https://orcid.org/0000-0002-1472-1138>

Grégoire Misguich  <https://orcid.org/0000-0002-7012-3204>

References

- [1] Baxter R J 2007 *Exactly Solved Models in Statistical Mechanics* (New York: Dover)
- [2] Bertini B, Collura M, De Nardis J and Fagotti M 2016 Transport in out-of-equilibrium XXZ chains: exact profiles of charges and currents *Phys. Rev. Lett.* **117** 207201

¹⁴The time variables t and t' are respectively associated to the dynamics with κ and κ' .

- [3] Bethe H A 1931 Zur theorie der metalle: I. Eigenwerte und eigenfunktionen der linearen atomkette *Z. Phys.* **71** 205–31
- [4] Bulchandani V B 2017 On classical integrability of the hydrodynamics of quantum integrable system *J. Phys. A: Math. Theor.* **50** 435203
- [5] Castro-Alvaredo O A, Doyon B and Yoshimura T 2016 Emergent hydrodynamics in integrable quantum systems out of equilibrium *Phys. Rev. X* **6** 041065
- [6] Croydon D A, Kato T, Sasada M and Tsujimoto S 2018 Dynamics of the box-ball system with random initial conditions via Pitman’s transformation (arXiv:1806.02147)
- [7] Croydon D A and Sasada M 2019 Invariant measures for the box-ball system based on stationary Markov chains and periodic Gibbs measures *J. Math. Phys.* **60** 083301
- [8] Croydon D A and Sasada M 2020 Generalized hydrodynamic limit for the box-ball system (arXiv:2003.06526)
- [9] De Nardis J, Bernard D and Doyon B 2018 Hydrodynamic diffusion in integrable systems *Phys. Rev. Lett.* **121** 160603
- [10] De Nardis J, Bernard D and Doyon B 2019 Diffusion in generalized hydrodynamics and quasiparticle scattering *SciPost Phys.* **6** 049
- [11] Doyon B 2019 Lecture notes on generalized hydrodynamics (arXiv:1912.08496)
- [12] Doyon B and Spohn H 2017 Dynamics of hard rods with initial domain wall state *J. Stat. Mech.* **073210**
- [13] Doyon B, Yoshimura T and Caux J-S 2018 Soliton gases and generalized hydrodynamics *Phys. Rev. Lett.* **120** 145301
- [14] El G A 2003 The thermodynamic limit of the Whitham equations *Phys. Lett. A* **311** 374
- [15] El G A and Kamchatnov A M 2005 Kinetic equation for a dense soliton gas *Phys. Rev. Lett.* **95** 204101
- [16] El G A, Kamchatnov A M, Pavlov M V and Zykov S A 2011 Kinetic equation for a soliton gas and its hydrodynamic reductions *J. Nonlinear Sci.* **21** 151–91
- [17] Fendley P and Saleur H 1996 Nonequilibrium dc noise in a Luttinger liquid with an impurity *Phys. Rev. B* **54** 10845
- [18] Ferrari P A and Gabrielli D 2018 BBS invariant measures with independent soliton components (arXiv:1812.02437)
- [19] Ferrari P A, Nguyen C, Rolla L T and Wang M 2018 Soliton decomposition of the Box-Ball System (arXiv:1806.02798)
- [20] Fukuda K, Okado M and Yamada Y 2000 Energy functions in box ball systems *Int. J. Mod. Phys. A* **15** 1379–92
- [21] Gopalakrishnan S, Huse D A, Khemani V and Vasseur R 2018 Hydrodynamics of operator spreading and quasiparticle diffusion in interacting integrable systems *Phys. Rev. B* **98** 220303(R)
- [22] Gopalakrishnan S and Vasseur R 2019 Kinetic theory of spin diffusion and superdiffusion in XXZ spin chains *Phys. Rev. Lett.* **122** 127202
- [23] Inoue R, Kuniba A and Takagi T 2012 Integrable structure of box-ball systems: crystal, Bethe ansatz, ultradiscretization and tropical geometry *J. Phys. A: Math. Theor.* **45** 073001
- [24] Kamchatnov A M 2000 *Nonlinear Periodic Waves and Their Modulations: An Introductory Course* (Singapore: World Scientific)
- [25] Kuniba A and Lyu H 2020 Large deviations and one-sided scaling limit of randomized multicolor box-ball system *J. Stat. Phys.* **178** 38–74
- [26] Kuniba A, Nakanishi T and Tsuboi Z 2002 The canonical solutions of the Q-systems and the Kirillov–Reshetikhin conjecture *Commun. Math. Phys.* **227** 155–90
- [27] Kuniba A and Takagi T 2010 Bethe ansatz, inverse scattering transform and tropical Riemann theta function in a periodic soliton cellular automaton for $A_n^{(1)}$ *SIGMA* **6** 52
- [28] Kuniba A, Takagi T and Takenouchi A 2006 Bethe ansatz and inverse scattering transform in a periodic box-ball system *Nucl. Phys. B* **747** 354–97
- [29] Levine L, Lyu H and Pike J 2017 Double jump phase transition in a soliton cellular automaton (arXiv:1706.05621)
- [30] Lewis J, Lyu H, Pylyavskyy P and Sen A 2019 Scaling limit of soliton lengths in a multicolor box-ball system (arXiv:1911.04458)
- [31] Takahashi D 1993 On some soliton systems defined by using boxes and balls *Proc. of the Int. Symp. on Nonlinear Theory and Its Applications (NOLTA '93)* pp 555–8
- [32] Takahashi D and Matsukidaira J 1997 Box and ball system with a carrier and ultradiscrete modified KdV equation *J. Phys. A* **30** L733–9

- [33] Takahashi D and Satsuma J 1990 A soliton cellular automaton *J. Phys. Soc. Japan* **59** 3514–9
- [34] Takahashi M 1999 *Thermodynamics of One-Dimensional Solvable Models* (Cambridge: Cambridge University Press)
- [35] Tsarëv S P 1991 The geometry of Hamiltonian systems of hydrodynamic type. The generalized hodograph method *Math. USSR Izvestiya* **37** 397
- [36] Yang C N and Yang C P 1969 Thermodynamics of a one-dimensional system of bosons with repulsive delta-function interaction *J. Math. Phys.* **10** 1115–22
- [37] Yoshihara D, Yura F and Tokihiro T 2003 Fundamental cycle of a periodic box-ball system *J. Phys. A: Math. Gen.* **36** 99–121
- [38] Zakharov V E 1971 Kinetic equation for solitons *J. Exp. Theor. Phys. Lett.* **33** 538